Prediction of Noise-Power-Distance Data for Urban Air Mobility Vehicles

Stephen A. Rizzi, Stefan J. Letica, D. Douglas Boyd, Jr. and Leonard V. Lopes
NASA Langley Research Center, Hampton, VA 23681

In contrast to most commercial air traffic today, vehicles serving the urban air mobility (UAM) market are anticipated to operate within communities and be close to the public at large. The approved model for assessing environmental impact of air traffic actions in the United States, the Federal Aviation Administration Aviation Environmental Design Tool (AEDT), does not directly support analysis of such operations due to a combined lack of UAM aircraft flight performance model data and aircraft noise data. This paper addresses the latter by offering two prediction-based approaches for generation of noise–power–distance data for use within AEDT. One utilizes the AEDT fixed-wing aircraft modeling approach, and the other utilizes the AEDT rotary-wing aircraft modeling approach.

Nomenclature

B	=	regression coefficient
c	=	speed of sound in air, ft/s or m/s
d	=	slant range distance, ft or m
F_x, F_y, F_z	=	forces in the x, y, and z directions, lbf or N
L_A	=	A-weighted sound pressure level, dBA
L_{AE}	=	A-weighted sound exposure level, dBA
L_{EPN}	=	effective tone-corrected perceived noise level, EPNdB
L_{TPN}	=	tone-corrected perceived noise level, PNdB
M	=	Mach number
MN_{ADJ}	=	source noise adjustment due to advancing tip Mach number, dB
R	=	blade length, ft or m
r	=	radius, ft or m
T	=	temperature, °F or °C
V	=	airspeed, knots or km/h
τ_x, τ_y, τ_z	=	moments in the x, y, and z directions, lbf · ft or N · m
ω	=	rotational speed, revolutions/min or Hz

Subscripts

ADV	=	rotor advancing side
mx	=	maximum
R	=	reference condition
T	=	operating condition
x, y, z	=	Cartesian axes

I. Introduction

THE internationally recommended integrated noise modeling method for fixed-wing aircraft is detailed in International Civil Aviation Organization (ICAO) Doc 9911 [1] (see also the European Civil Aviation Conference Doc 29 [2]). In the United States, the Federal Aviation Administration (FAA) Aviation Environmental Design Tool (AEDT) [3] is the required tool to assess aircraft noise and other environmental impacts due to federal actions at civilian airports, vertiports, or in U.S. airspace for commercial flight operations. The noise, aircraft flight profile, and flight path computational methods implemented in AEDT are compliant with Doc 9911. Therefore, the capabilities for, and limitations of, analysis of fixed-wing aircraft in AEDT are the same or similar to those of other Doc 9911–compliant programs. Doc 9911–compliant computer programs calculate various noise metrics using noise–power–distance (NPD) data specific to each aircraft. In the customary mode of operation, a flight performance model determines the engine power required to execute the specified flight operation. A key assumption is that noise levels are highly correlated with the corrected net thrust of the engines. This allows noise data to be interpolated for power and distance, along with various other adjustments, to estimate the sound exposure at a set of receptors on the ground.

There are no international standards for modeling rotary-wing (helicopter) aircraft using integrated modeling methods. AEDT supports rotary-wing noise analyses by supplementing the fixed-wing noise databases with rotary-wing NPD data and by providing support for helicopter operational modes. It calculates sound exposure using noise–mode–distance (still termed NPD) data specific to the vehicle's operational mode, e.g., vertical ascent. The noise data are interpolated for distance only and are used, with adjustments, to estimate the sound exposure at a set of ground receptors. There is no equivalent correlating parameter such as corrected net thrust.

There are some obstacles to using integrated modeling methods for assessment of community noise due to urban air mobility (UAM) vehicle operations. The first is that while there are NPD data for existing fixed-wing vehicles in the databases used in Doc 9911–compliant programs (and for existing rotary-wing vehicles in AEDT), there are no available NPD data for UAM vehicles, whether the vehicles are modeled as fixed-wing-type or rotary-wing-type vehicles. Secondly, when modeling a UAM vehicle as a fixed-wing type, there are no performance data available to determine required engine power, nor is it clear that engine power is a good predictor of noise. When modeling a UAM vehicle as a rotary-wing type, the defined operating modes within AEDT are limited to a few that are appropriate for typical helicopter operations but that may be insufficient for describing UAM operations.

A recent white paper [4] established a set of high-level goals to address key issues associated with UAM noise. One of these goals is to examine UAM fleet noise impacts through prediction and measurement, along with a recommendation that "Research be conducted to more fully explore limitations in methods for assessing community noise impact of UAM vehicles in their operational environments, and to generate a software development plan that addresses the limitations of current models over time." To that end, this paper describes two approaches for generating UAM vehicle NPD data. Both approaches are based on source noise predictions using the NASA

Presented as Paper 2022-2839 at the 28th AIAA/CEAS Aeroacoustics Conference, Southampton, England, U.K., June 14–17, 2022; received 9 March 2023; revision received 10 June 2023; accepted for publication 26 August 2023; published online 5 October 2023.

*Senior Researcher for Aeroacoustics, Aeroacoustics Branch; stephen.a.rizzi@nasa.gov. Fellow AIAA (Corresponding Author).

†Research Engineer, Aeroacoustics Branch; stefan.j.letica@nasa.gov.

‡Senior Research Engineer, Aeroacoustics Branch; d.d.boyd@nasa.gov. Senior Member AIAA.

§Senior Research Engineer, Aeroacoustics Branch; leonard.v.lopes@nasa.gov.

second-generation Aircraft Noise Prediction Program (ANOPP2) [5]. One approach is directed at generating NPD data suitable for modeling UAM vehicles as fixed-wing types in Doc 9911–compliant programs, including AEDT. The other approach is directed at generating NPD data for modeling UAM vehicles as rotary-wing types specifically using AEDT. The first generation (Gen 1) fixed-wing NPD database contained periodic loading and thickness noise for two UAM reference vehicles [6]. The second generation (Gen 2) fixed-wing NPD database added broadband self-noise [7]. In this work, updates to the Gen 2 source noise data serve as the basis for a third-generation (Gen 3) NPD database for fixed-wing and rotary-wing type vehicles. The updates to the source noise data include the addition of metadata for tracking and maintaining source data pedigree, utilization of a consistent (lossless) treatment of atmospheric absorption for periodic and broadband noise components, and a means to export data to a self-describing file format (as discussed in the Supplemental Material accompanying this paper; see Appendix). The updates to the NPD data include use of a new tool that allows generation of both fixed-wing-type and rotary-wing-type NPD data, as described in Sec. IV. The set of source noise and NPD data described herein is referred to as Gen 3.1.2.

II. Concept Vehicles and Operating States

A. Vehicle Description

Two reference vehicles developed under the NASA Revolutionary Vertical Lift Technology (RVLT) Project are included in this investigation, namely, the quadrotor and lift plus cruise (L+C) vehicles (see Fig. 1). Both vehicles are sized for a 1200 lb. (544 kg) payload (up to six passengers) executing a representative mission profile [8]. The quadrotor is an all-electric variant, with four three-bladed rotors, gross weight of 6469 lb. (2934 kg), and maximum airspeed V_{mx} of 109 knots true airspeed (KTAS) (202 km/h). The L+C is a turbo-electric variant, with eight two-bladed lifting rotors, a three-bladed pusher propeller, gross weight of 5903 lb. (2678 kg), and V_{mx} of 123 KTAS (228 km/h). Additional details on these configurations can be found in Ref. [9].

B. Operating States

Trajectory data from a set of operational scenarios with multiple vertiports were used in the Gen 1 and Gen 2 analyses. These data were reduced to determine aircraft operational states for which noise estimates are needed. As in the prior works [6,7], the aircraft operating states are defined by pairs of airspeed (knots) and climb angle (degrees). These comprise 42 and 44 unique operating states for the quadrotor and L+C vehicles, respectively, and are binned in 10-knot increments of airspeed (from 0 to 85% of V_{mx}) and in 5° increments of climb angle (from −90° in vertical descent to 90° in vertical ascent). Because the source noise prediction process can be computationally intensive, only those operating states having at least 10 occurrences in the Gen 1 trajectory data were evaluated. The set of Gen 1 operating states was compared with operating state data derived from the Gen 2 trajectory data and was found to adequately cover the range of conditions (see Fig. 2). Source noise data for operating states with airspeeds less than 5 knots were computed with zero airspeed, irrespective of climb angle.

For the Gen 3 NPD database, an additional operating state corresponding to the rotary-wing "Flight Idle" operational mode is required for both vehicles (see Sec. IV.B). Although not occurring in the Gen 1 or Gen 2 trajectory data, either this state or the "Ground Idle" state is required in the database for modeling rotary-wing departure and approach profiles within AEDT.

III. Source Noise Prediction Process

This section reviews the process for generating source noise data through analysis, including determination of trimmed conditions for each vehicle. The source noise data are subsequently used for

Fig. 1 NASA RVLT reference vehicle configurations considered in this study: quadrotor (left) and lift plus cruise (right).

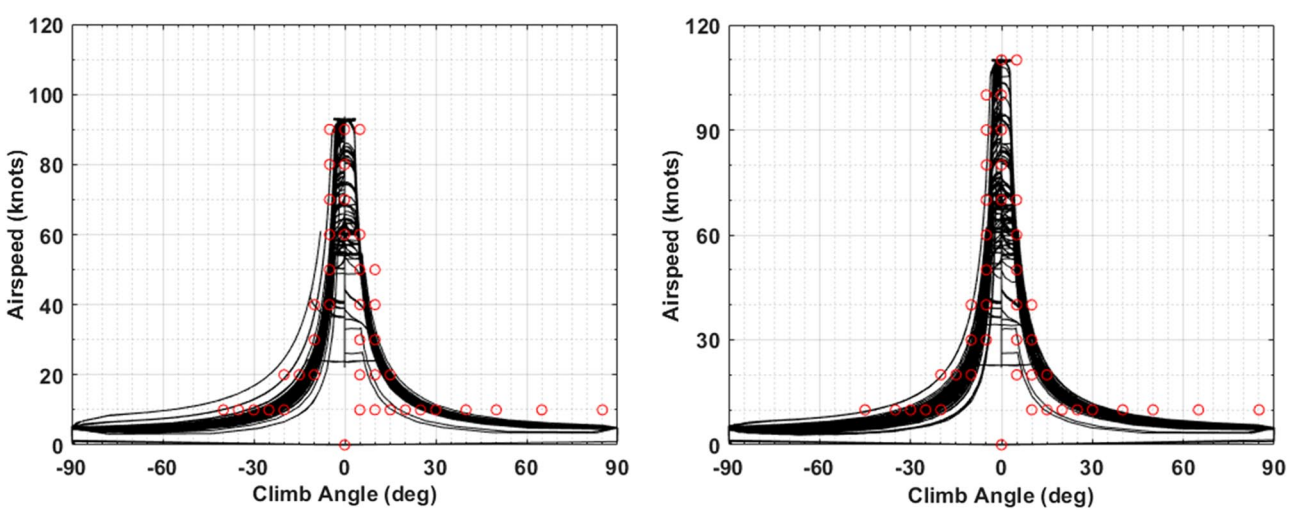

Fig. 2 Operating states for the quadrotor (left) and L+C (right) vehicles. Black lines represent Gen 2 trajectory data, and red circles represent operating states identified in the Gen 1 study.

generation of both fixed-wing and rotary-wing NPD data. A summary of each analysis step follows. The overall process is depicted in Fig. 3, in which the script "pyaaron" executes all steps for each operating state.

A. Vehicle Trim

For a given vehicle (quadrotor or L+C) and prescribed operating state, the vehicle is "trimmed" in an iterative process using a comprehensive analysis code. For this work, the Comprehensive Analytical Model of Rotorcraft Aerodynamics and Dynamics (CAMRAD II) [10] computer program is used to trim the vehicles. In the trimmed condition, the control surface configuration of the vehicle corresponds to the desired operating state (airspeed and climb angle). CAMRAD II provides the lifting line geometry and motion to both the compact loading and compact thickness models, and the forces acting on the lifting line to the compact loading model (see Sec. III.B). CAMRAD II also provides the angle of attack and the three components of wake-induced fluid velocity as a function of rotor blade radial station and azimuth. These serve as inputs to source noise prediction modules explained below. It should be noted that the simplest trim strategies were adopted in this work. Because these vehicles have redundant controls, e.g., lifting rotors and wings for lift, there may be multiple ways to trim the vehicle to a prescribed operating state and the noise produced by each generally differ. Optimization of trim strategies for low noise is an active area of research and is beyond the scope of this paper.

1. *Quadrotor Vehicle Trim*

The rotors on the quadrotor vehicle operate at a constant rotational speed with a 20 Hz blade passage frequency (BPF) and the vehicle was designed to utilize collective pitch control. The six trim targets for the six-degree-of-freedom (6-DOF) trim are the three net forces and three net moments (F_x, F_y, F_z, τ_x, τ_y, and τ_z) in the aircraft coordinate system acting on the aircraft center of gravity (CG). Four of the six trim variables are four pilot controls: collective stick, lateral stick, longitudinal stick, and pedal. These pilot controls (variables) are connected to appropriate combinations of the four rotors' collective pitch settings. The remaining two trim variables involve two vehicle orientation angles: vehicle pitch and vehicle roll. This same 6-DOF trim method is used for all speed and climb angle combinations. For flight idle (used when modeling aircraft in AEDT as rotary-wing vehicles), the vehicle rests on the ground and the net vertical force F_z is trimmed to 80% of the vehicle weight with the trim variable being pilot collective stick. Lacking a standard, engineering judgment was used to set that level such that it was greater than ground idle and less than hover. All other motion of the vehicle is restricted to zero. Furthermore, the ground effect model of CAMRAD II is enabled. This model incorporates the effect of the ground on the free wake geometry by using an image plane and the effect of one rotor's wake on the others. This free wake geometry, altered by the presence of the ground and the other rotors as shown in Fig. 4, affects the trim and blade loading. In this figure, the front rotors are shown in blue, the aft rotors are shown in red, and the positive z direction is down.

2. *L+C Vehicle Trim*

The lifting rotors and pusher propeller on the L+C vehicle also operate at a constant rotational speed (35 Hz BPF for lifting rotors, 127 Hz BPF for propeller) and the vehicle was designed to utilize collective pitch control. However, different trim variables and trim targets are used depending on the flight conditions. At low speeds, the

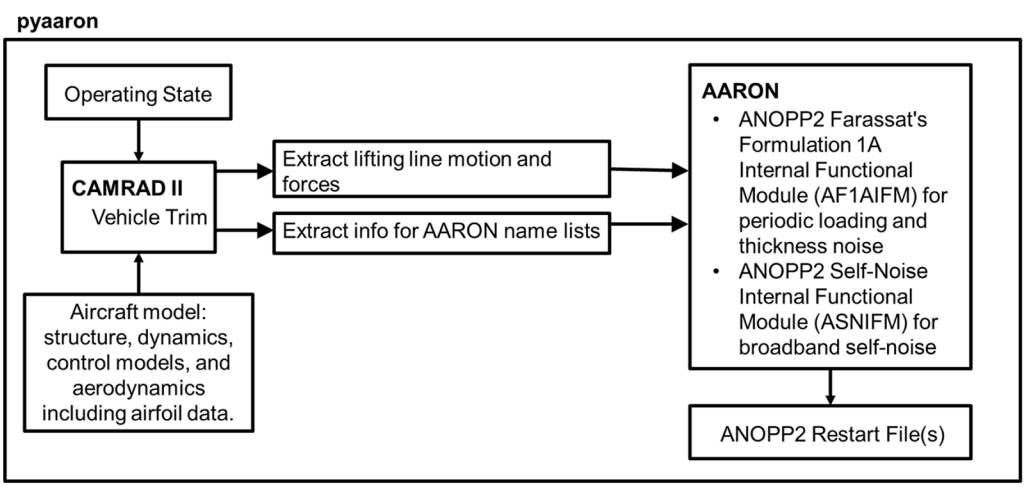

Fig. 3 NASA process for generating source noise data for each operating state.

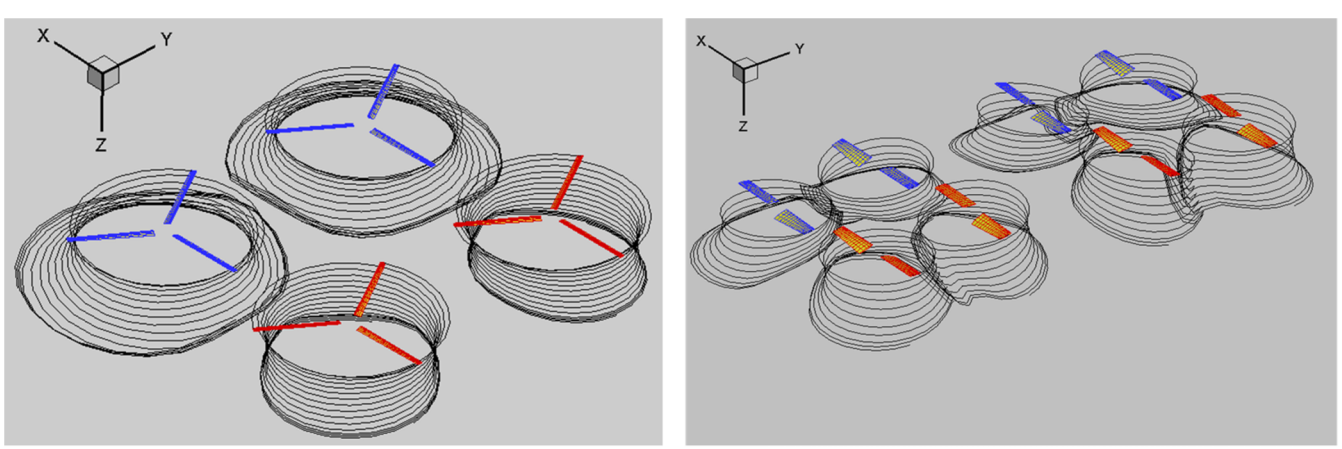

Fig. 4 Interaction of free wakes with ground plane and with each other for quadrotor (left) and L+C vehicles (right) in ground idle mode.

pusher propeller is not used as a trim variable. The trim targets are three degrees of freedom for longitudinal trim (F_x, F_z, and τ_y). Two of the three trim variables are pilot controls: collective stick and longitudinal stick; the third trim variable is the vehicle pitch angle. At moderate speeds, all lifting rotors and the pusher propeller are active. The trim targets are the same as those used at low speed; however, the third trim variable is the pusher collective pitch instead of the vehicle pitch orientation. In this case, the vehicle pitch orientation is set to zero. At high-speed (cruise) conditions, the lifting rotors are turned off and the wing produces lift, with thrust provided by the pusher propeller. The trim targets are two degrees of freedom for longitudinal trim (F_x and F_z), and trim variables include the pusher collective pitch and vehicle pitch orientation. The dividing lines between trim modes are determined by several factors related to the operating state. For flight idle, the vehicle is trimmed in ground effect in the same manner as the quadrotor vehicle except that, like the low-speed scheme, the pusher propeller is not used. Wake interactions are shown in Fig. 4.

B. Source Noise Definition

Source noise data are generated using the ANOPP2 Aeroacoustic Rotor Noise (AARON) tool. Two noise sources are included in the Gen 3 database, namely, combined periodic loading and thickness noise, and broadband self-noise. Farassat's Formulation 1A [11], incorporated in the ANOPP2 Formulation 1A Internal Functional Module (AF1AIFM) [12], is used to compute the combined periodic loading and thickness noise under each quasi-static operating condition. For all source noise calculations in this paper, the compact thickness and compact loading version of AF1AIFM is used [13]. For compact thickness, the user provides the cross-sectional area of the blade section as a function of blade radius. In pyaaron, the user provides the maximum thickness-to-chord ratio at radial stations, and the cross-sectional area is computed assuming an NACA 00XX airfoil section, where XX is the thickness-to-chord ratio in percent. CAMRAD II input, discussed in Sec. III.A, is used for compact loading noise computations.

Broadband self-noise data are generated using the ANOPP2 Self-Noise Internal Functional Module (ASNIFM), following the semi-empirical formulations in Ref. [14]. Additional input data for the self-noise analyses, apart from the CAMRAD II output, include the zero-lift angle of attack as a function of rotor radius and the trailing edge (TE) thickness and the TE wedge angle as a function of rotor radius. The vehicle sizing process using the NASA Design and Analysis of Rotorcraft (NDARC) code [15] specified the lifting rotor and cruise propeller blades to use a Sikorsky SSC-A09 rotorcraft airfoil table for the inboard section ($0 \le r/R \le 0.85$) and a Boeing-Vertol VR-12 rotorcraft airfoil table for the outboard section ($0.95 \le r/R \le 1$), with an interpolation between those airfoil tables for intermediate stations ($0.85 \le r/R \le 0.95$). The zero-lift angle, shown in Fig. 5, was calculated under a hover condition as a function of Mach number at each radial station. The sensitivity of the self-noise calculation to the zero-lift angle has not been thoroughly investigated, so no effort was undertaken as part of this study to incorporate an azimuthal variation that would accompany any of the forward flight conditions. The TE thicknesses and wedge angles were not specified as part of the NDARC or CAMRAD II analyses. A constant TE thickness (scaled by rotor radius) and a constant TE wedge angle were specified based on representative data from the HART II rotor [16] (see Table 1). Because the self-noise calculation is known to be sensitive to these TE parameters, the resulting self-noise data are not considered to be generally applicable to other airfoil geometries.

Source noise data generated by AARON for each operating state are provided on a hemisphere of observers centered about the CG of each vehicle at 10° increments in polar angle (fore-aft) and azimuthal angle (port-starboard) and at a radius of 500 ft (152 m). This radius, corresponding to 100 times the lifting rotor radii of the L+C vehicle and about 38 times the rotor radii of the quadrotor vehicle, was selected to ensure that the hemisphere contained only far-field noise. The set of observers on the hemisphere moves with the vehicle and, therefore, does not include the Doppler frequency shift that would be experienced by a stationary ground observer. The source noise data are written to ANOPP2 restart files for subsequent calculation of NPD data. Example loading and thickness noise and broadband self-noise data for the quadrotor vehicle are shown in Fig. 6 for a high-speed cruise condition. In this figure, the nose is in the positive x direction, and the positive z direction is up. The combined loading and thickness noise is highly directional, whereas the broadband self-noise is more uniformly distributed and is characterized by an overall dipole shape.

Source noise hemisphere data for all operating conditions are provided in the Supplemental Material that accompanies this paper (see Appendix).

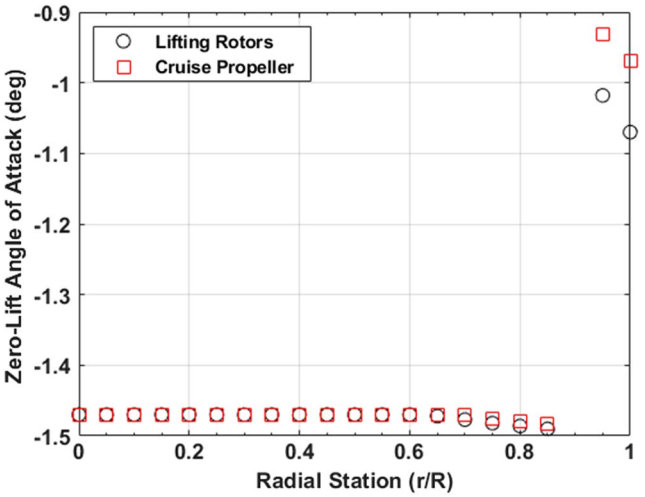

Fig. 5 Zero-lift angle of attack used in the calculation of the broadband self-noise component.

Table 1 Additional parameters used in the calculation of the broadband self-noise component

Rotor	TE thickness, in. (mm)	TE wedge angle, deg
Quad lifting rotor	0.071 (1.8)	18
L+C lifting rotor	0.027 (0.69)	18
L+C cruise propeller	0.024 (0.62)	18

IV. Noise–Power–Distance Data Generation

The notion of deriving NPD data from computational analysis is not new. The authors of Ref. [17] developed a framework for calculating NPD data for novel fixed-wing aircraft by considering changes in aircraft technology and/or operations to a baseline vehicle and operating condition. In contrast, NPD data in the present work are generated in an absolute sense, i.e., not as a change to a baseline vehicle and operating condition. Further, all NPD data for the quadrotor and L+C vehicles, whether represented as the fixed-wing aircraft type or the rotary-wing aircraft type, are derived from the same set of source noise data. In the typical AEDT analysis, each set of NPD data consists of a set of noise metrics as a function of distance and power (fixed wing) or operational mode (rotary wing). For fixed-wing aircraft and rotary-wing aircraft in dynamic operational modes (see Sec. IV.B), these include maximum metrics (the maximum A-weighted sound pressure level L_{Amx} and the maximum tone-corrected perceived noise level L_{TPNmx}), and time-integrated exposure metrics (the A-weighted sound exposure level L_{AE} and the effective tone-corrected perceived noise level L_{EPN}). For rotary-wing aircraft in static operational modes, these include only the maximum metrics, with exposure metrics calculated within AEDT based on the user-specified duration. Each metric is calculated at reference distances (the "distance" in NPD) of d = 200, 400, 630, 1k, 2k, 4k, 6.3k, 10k, 16k, and 25k ft (61, 122, 192, 305, 610, 1.22k, 1.92k, 3.05k,

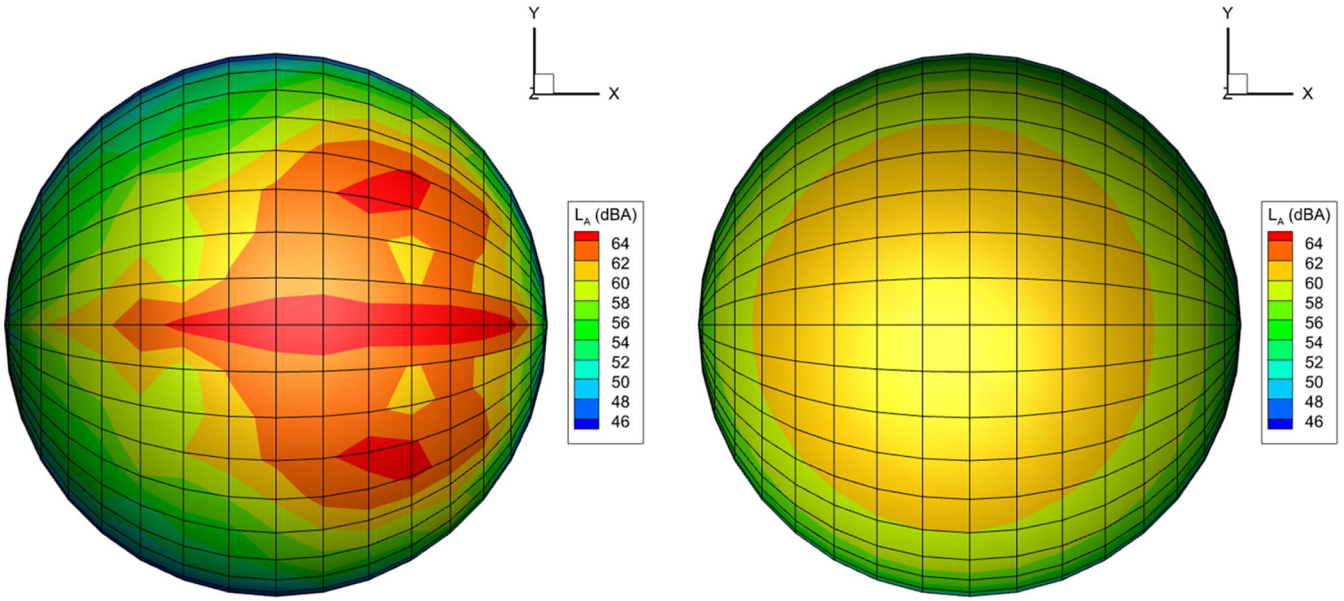

Fig. 6 A-weighted overall sound pressure level (L_A) of quadrotor combined loading and thickness noise (left) and broadband self-noise (right) for high-speed cruise.

4.88k, and 7.62k m). Note that the reference distances reflect the slant range between the source and the receiver. The different processes for NPD data generation used for the different aircraft types are discussed next.

A. Fixed-Wing Aircraft

AEDT permits an NPD data set for each of its three fixed-wing operational modes (approach, departure, and level flight). Other Doc 9911–compliant programs may not make the distinction for level flight. In a typical fixed-wing analysis, a set of procedural steps is used to specify an aircraft operation. For example, a standard approach operation is constructed as a sequence of "descent" procedural steps with increasing flap deployment and decreasing speed, followed by "landing" and "deceleration" steps. AEDT uses one of its performance models to determine the corrected net thrust per engine (the "power" in NPD) required for each procedural step and constructs a flight profile consisting of the distance along the ground track, the aircraft altitude, the aircraft true airspeed, and the corrected net thrust. The aircraft altitude is referenced to field elevation for approach and departure modes, and to mean sea level for the level flight mode. Doc 9911–compliant programs interpolate NPD data on power and distance, and apply various adjustments [3] to determine the noise at a set of ground receptors. This approach does not work well for UAM aircraft because flight performance model data do not exist in the ICAO Aircraft Noise and Performance (ANP) [18] and Base of Aircraft Data Family 3 (BADA 3) [19] databases used in Doc 9911–compliant programs.

An alternative modeling methodology available in Doc 9911–compliant programs and employed in the prior UAM studies [6,7] directly specifies the flight profile (so-called fixed-point flight profiles), bypassing the need for a performance model to determine the power for each procedural step. In that usage, a unique identifier corresponding to the operating state (function of airspeed and climb angle) is used in place of power to designate each NPD data set. This approach requires as many NPD data sets as there are operating states, and care is needed in this approach to minimize the effect of unwanted interpolation of NPD data between unrelated operating states [6].

When using fixed-point flight profiles, the computational process used to generate fixed-wing NPD data for each operating state is shown in Fig. 7. Following the loading of an ANOPP2 restart file (containing the source noise data associated with a single operating state), Doppler frequency shift is applied using the ANOPP2 Wind Tunnel and Flight Effects Internal Functional Module (AWTFEIFM). For each AEDT reference distance, the resulting data are propagated to a 4-ft-(1.2-m)-height centerline microphone location using the ANOPP2 Straight Ray Propagation Internal Functional Module (ASRPIFM). The source noise data are "flown" via simulation along a straight and level flight path at the AEDT reference speed of 160 knots (296 km/h), irrespective of the flight speed and climb angle associated with the particular operational state, as depicted in Fig. 8. By specifying uniform atmospheric conditions, different slant range distances d may be computed by a simple change in altitude. A receiver time interval of 0.5 s is used in ASRPIFM to generate a set of one-third octave band spectral data at the ground observer, and noise metrics are calculated using the ANOPP2 Acoustic Analysis Utility (AAAU). In this application, AAAU is set to include tones below 800 Hz in the calculation of L_{TPN} (and hence L_{EPN}) because of the low blade passage frequencies of both vehicles. The process depicted in Fig. 7 is incorporated into the ANOPP2 Mission Analysis Tool (AMAT).

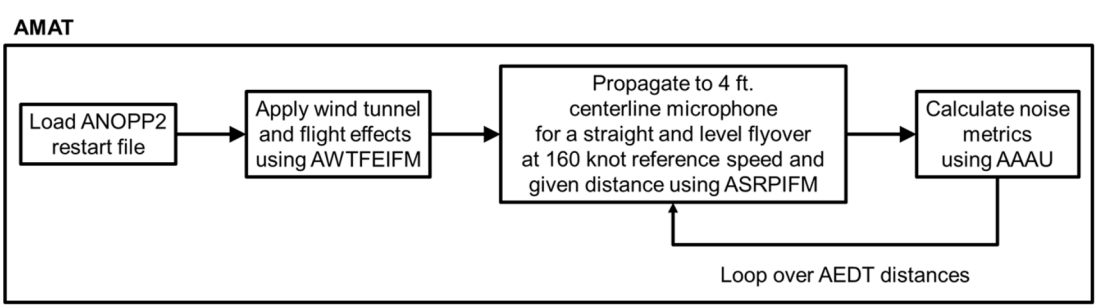

Fig. 7 Computational steps in AMAT for generating fixed-wing NPD data for each operating state.

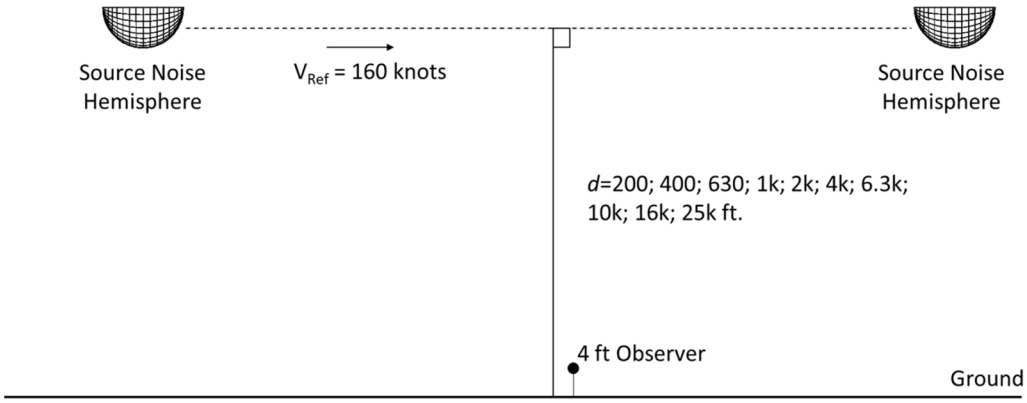

Fig. 8 Simulation scenario for generating fixed-wing NPD data for each operating state.

In this work, ASRPIFM employs the SAE ARP 866A [20] atmospheric absorption model, using the Chien–Soroka ground plane reflection model [21] with the Delany–Bazley finite impedance model [22] for soft ground. In the current implementation, AMAT uses the single emission angle approach in which the directivity angles associated with the ground-reflected ray are the same as those associated with the direct ray, and spherical spreading and atmospheric absorption are the same for both ground-reflected and direct rays [5]. The infinitely long flight path assumed by the path segmentation modeling approach [1] is effectively achieved by ensuring that the finite path length used in the simulation is sufficiently long to obtain both the maximum level metrics and the time-integrated exposure metrics between the 10 dB down points on either side of the maximum level. For the latter, the minimum simulation path length increases with increasing distance. Along with other noise adjustments, speed adjustments are applied to the exposure metrics to compensate for the difference between the fixed-wing reference speed of 160 knots (296 km/h) and the airspeed associated with the particular operating state [3].

While AEDT v3d and above allow user-specified spectral data and while the computational approach described herein can generate such data, no attempt to do so is made in this work. Consequently, AEDT metric calculations and adjustments requiring the use of spectral data, e.g., C-weighted metrics or changes to atmospheric absorption type, should not be undertaken.

It should be noted that the NPD data generation method described above, in essence, follows that of SAE AIR 1845A [23] using the "integrated procedure" with Type 1 data. However, instead of measuring one set of NPD data at a nominal distance between 328 and 2625 ft (100 and 800 m) and extrapolating to the other reference distances (per AIR 1845A), the current method directly computes the data at all reference distances. This avoids use of the "simplified adjustment procedure" in AIR 1845A for extrapolation to distances greater than 2625 ft (800 m). The simplified procedure employs an empirically derived duration adjustment that likely does not apply to UAM vehicles and assumes that the emission angle corresponding to L_{Amx} is unchanged for distances greater than 2625 ft (800 m).

B. Rotary-Wing Aircraft

This subsection pertains only to the generation of rotary-wing NPD data for use in AEDT, as rotary-wing analysis capabilities do not generally exist in other Doc 9911–compliant programs. In contrast to fixed-wing aircraft, in which flight profile data can be input either through a set of procedural steps or as fixed points, AEDT flight profile data for rotary-wing aircraft can only be specified through a set of procedural steps. These procedural steps are similar to fixed-wing, fixed-point flight profiles in that they do not require a flight performance model. Each procedural step denotes a particular operational mode. For example, a simple departure operation may be constructed from the following sequence of operational mode procedural steps: ground idle → flight idle → vertical ascent → departure with climbing acceleration → level flyover with constant speed. The noise data are specified as a function of operational mode (instead of power) and distance, though are still referred to as NPD data. As is the case for the fixed-wing NPD data described above, there are as many rotary-wing NPD data sets as there are operational modes. However, because rotary-wing NPD data are not interpolated between operational modes, the measures taken in prior work [6,7] to minimize the effect of interpolation between unrelated fixed-wing NPD data sets are not needed.

AEDT rotary-wing operational mode procedural steps are classified as either dynamic or static (see Table 2). AEDT will substitute modes (in some cases with mode-specific dB adjustments) for those that are missing from the NPD database, as indicated in the rightmost column in Table 2. Given that manufacturer-supplied rotary-wing NPD data in AEDT are typically limited to the minimum set of five operational modes, i.e., modes A, D, L, G or H, and I or J, with 0 dB mode-specific adjustments for missing modes, only those modes and adjustments are considered herein. Even if all 16 operational modes were supplied, it is immediately apparent that some condensation of source noise data from the 40+ operating states identified above is required. Casting of the 40+ operating states shown in Fig. 2 into a relatively small number of allowable rotary-wing operational modes is driven, in part, by condensation considerations, which are treated differently depending on the mode. There exists a shortcoming in modeling the noise of flights having many different operating states when using rotary-wing NPD because of its limited operational modes. In contrast, there is no limit to the number of fixed-wing NPD data that may be used.

It should be noted that unlike the methods used for generating fixed-wing NPD data, essentially following AIR 1845A [23], there is no standard for generating rotary-wing NPD data. To the extent possible, the methods used herein are consistent with those for

Table 2 AEDT rotary-wing operational mode procedural steps

Operational mode	Description	State	Substitute mode
A	Approach at constant speed	Dynamic	—
B	Approach with horizontal deceleration	Dynamic	A + Adj.
C	Approach with descending deceleration	Dynamic	A + Adj.
D	Departure at constant speed	Dynamic	—
E	Depart with horizontal acceleration	Dynamic	D + Adj.
F	Depart with climbing acceleration	Dynamic	D + Adj.
L	Level flyover at constant speed	Dynamic	—
T	Taxi at constant speed	Dynamic	H/I
G	Ground idle	Static	H
H	Flight idle	Static	G
I	Hover in ground effect	Static	J
J	Hover out of ground effect	Static	I
V	Vertical ascent in ground effect	Static	I + Adj.
W	Vertical ascent out of ground effect	Static	J + Adj.
Y	Vertical descent in ground effect	Static	I + Adj.
Z	Vertical descent out of ground effect	Static	J + Adj.

helicopter certification according to 14 CFR Part 36 Appendix H [24].

1. *Dynamic Operational Modes*

The computational steps for generating rotary-wing NPD data for dynamic operational modes are similar to those of fixed wing, except for two important distinctions (see Fig. 9). One distinction is that, for each dynamic mode, three sets of noise metrics are needed as a function of the AEDT reference distances: one set along the centerline and one each at ±45° azimuth angles to represent lateral directivity (see Fig. 10). The lateral directivity adjustment in AEDT interpolates NPD data for lateral emission angles between ±45° and uses the data at ±45° for lateral emission angles greater than |±45°|. The additional observers require additional simulations because the trade of altitude for distance is different between the centerline observer and the lateral observers. The other distinction is that the NPDs are computed from a simulated flyover at the intended operating state (airspeed and climb angle), not at the reference airspeed of 160 knots (296 km/h) in level flight used for fixed-wing aircraft. There is a different reference speed for each dynamic operational mode A, D, and L.

a. Dynamic Mode L (Level Flyover at Constant Speed). Simulation of dynamic mode L for generation of NPD data is similar to the fixed-wing simulation, as depicted in Fig. 8. For both the quadrotor and L+C vehicles, there are multiple zero-climb-angle operating states having various nonzero airspeeds. The approach taken to condense the multiple cases down to a single mode L utilizes the AEDT source noise adjustment due to advancing tip Mach number (MN_{ADJ}). This adjustment, developed for helicopters, accounts for changes in sound level associated with changes in rotational speed, airspeed, and/or ambient temperature. This approach enables the mode L NPD to cover a range of flight speeds. The adjustment is described in 14 CFR Part 36 Appendix H [24] and examples are provided in Ref. [25]. The degree to which this adjustment applies to UAM vehicles, particularly in propeller-driven wing-borne flight, is discussed in Sec. V.B.

The approach is summarized as follows. First, at the 1000 ft (305 m) distance, values of L_{TPNmx} are calculated for each of the three observer locations for each of the nonzero airspeed level flight conditions. One of the airspeeds is selected as the reference airspeed for mode L. The source noise adjustment (MN_{ADJ} in ΔdB) for each of the three observers is given by

$$MN_{ADJ} = B_0 + B_1(M_{ADV_T} - M_{ADV_R}) + B_2(M_{ADV_T} - M_{ADV_R})^2 \tag{1}$$

in which B_0, B_1, and B_2 are vehicle-specific coefficients derived from a second-order polynomial regression of L_{TPNmx} as a function of ΔM_{ADV}, and M_{ADV}'s are the advancing tip Mach numbers at the operational and reference airspeeds V_T and V_R, respectively. M_{ADV} is the sum of the translational Mach number from the forward airspeed and the rotational blade tip Mach number, and it is given by

$$M_{ADV} = \left(1.688V + \frac{2\pi R\omega}{60}\right) \Big/ c \tag{2}$$

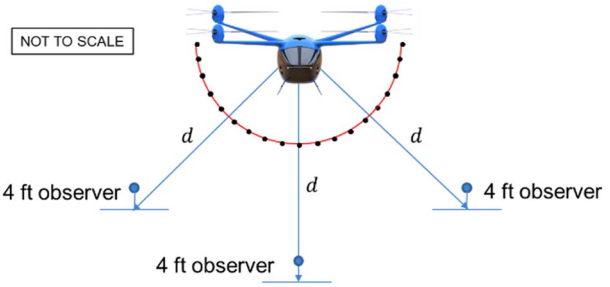

Fig. 10 Lateral distribution of observers (centerline, ±45°) for rotary-wing dynamic operational modes.

in which R is the blade length, ω is the rotational speed in revolutions per minute, and c is the speed of sound in air at a reference temperature T of 77°F (25°C). The NPD data for mode L is condensed to three sets (one for each observer) of noise metrics at the 10 AEDT reference distances for the selected reference condition, plus three sets of regression coefficients. The adjustments to the maximum noise levels and time-integrated noise exposure levels are applied within AEDT.

b. Dynamic Modes D (Departure at Constant Speed) and A (Approach at Constant Speed). Simulations of dynamic modes D and A for generation of NPD data are depicted in Figs. 11 and 12, respectively. Recalling Fig. 2, there are several departure operating states (having positive climb angles) and several approach operating states (having negative climb angles). The dividing line between operating states best characterized by static vertical ascent modes V/W with high climb angles and those best characterized by dynamic departure mode D with lesser climb angles lies in the realm of engineering judgment. The same argument holds for static vertical descent modes Y/Z and approach mode A. Even so, making such a distinction would still leave several operating states for each of modes D and A.

Unlike mode L, there is no advancing tip Mach number adjustment in AEDT that can aid in the condensation to a single set of NPD data for each of the modes D and A. The approach taken herein for the necessary condensation is simply to calculate metrics for every set of operating states identified as D and A, then to select one for each based on an appropriate criterion. For example, if a worst-case noise assessment was of interest, then the operating state having the highest levels could be selected. Alternatively, if a noise assessment of the average case was of interest, then the operating state best representing all NPD data could be selected. The average case was used in a recent paper [26] on modeling UAM community noise in AEDT rotary-wing mode. It is also feasible to perform a Monte Carlo simulation using many different vehicle variants of the same vehicle, each using a different distribution of NPD data. The important point is that only one set of data for each mode D and A can be specified per vehicle, and the set that is selected dictates the reference airspeed for the respective mode.

2. *Static Operational Modes*

The computational steps for generating rotary-wing NPD data for static operational modes differ from those used for fixed-wing and

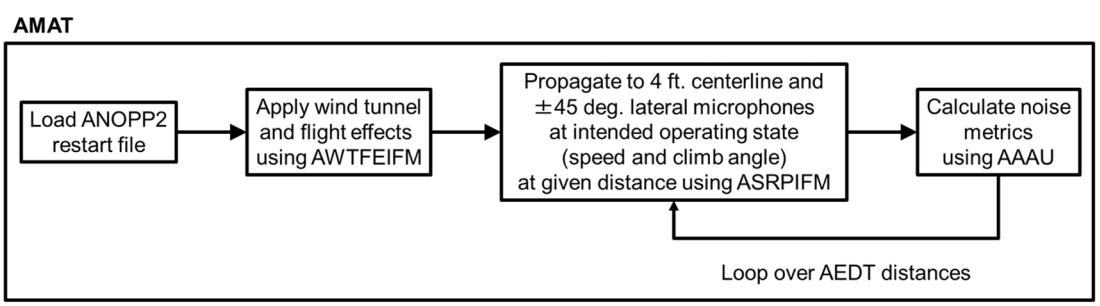

Fig. 9 Computational steps in AMAT for generating rotary-wing NPD data for dynamic operational modes A, D, and L.

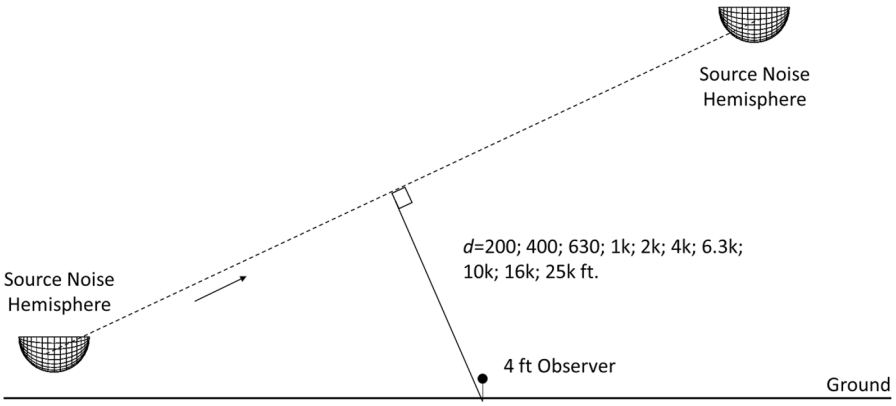

Fig. 11 Simulation scenario for generating rotary-wing NPD data for dynamic mode D.

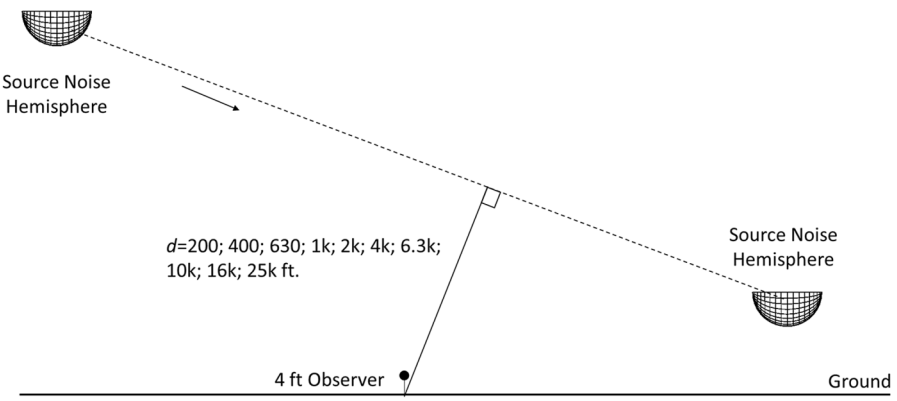

Fig. 12 Simulation scenario for generating rotary-wing NPD data for dynamic mode A.

dynamic rotary-wing data (see Fig. 13). Because the source and observer are stationary, there is no need to apply Doppler frequency shift before propagation. For each mode, a single set of maximum level noise metrics is computed as a function of the AEDT reference distances at locations directly in front of the vehicle. AEDT input for static modes includes a duration adjustment of the operation to calculate the time-integrated exposure metrics.

Vehicle and mode-specific directivity adjustments may also be provided. The adjustments are specified for a single ring of azimuthal observers (in 15–45° increments) as sound levels relative to the level directly ahead of the vehicle (see Fig. 14). When making ground measurements, these data are normally acquired at a 200 ft (61 m) radius. However, since the present data are being computed, consideration of azimuthal data at other radial distances is convenient, even if for no other purpose than to assess the variation in directivity with distance. If directivity adjustment data are not provided, a 0 dB adjustment is used, making the source effectively radiate as a monopole.

Directivity adjustment data may be specified separately for hard and soft ground. Note, however, that within AEDT, there are no means of selecting a ground type (hard or soft) for the static directivity adjustment independent of that used for the ground effect component of the lateral attenuation adjustment. This makes it impossible, e.g., to model a takeoff and landing at a hard surfaced vertiport while accounting for ground absorption along the route, without purposefully mislabeling hard ground directivity data as soft.

a. Static Modes G (Ground Idle) and H (Flight Idle). The methods for calculating NPD data for modes G and H are the same; it is only the source noise data that differ. Given that the aircraft of interest are electrically powered, the ground idle operational mode procedural step may not be applicable. Because AEDT rotary-wing departure and approach sequences must contain the Ground Idle step, it will be provided by way of substitution with the Flight Idle step. This additional operating state, particular to rotary-wing vehicles, augments the set of operating states used for fixed-wing analyses [6,7], as described in Sec. III.A. The corresponding source noise data were obtained with the ground effect model of CAMRAD II enabled (see Fig. 4).

In this work, mode H is calculated with the aircraft CG located at the height of the 4 ft (1.2 m) microphone, i.e., at a 0° elevation angle, with the top of the source noise hemisphere level with the microphone.

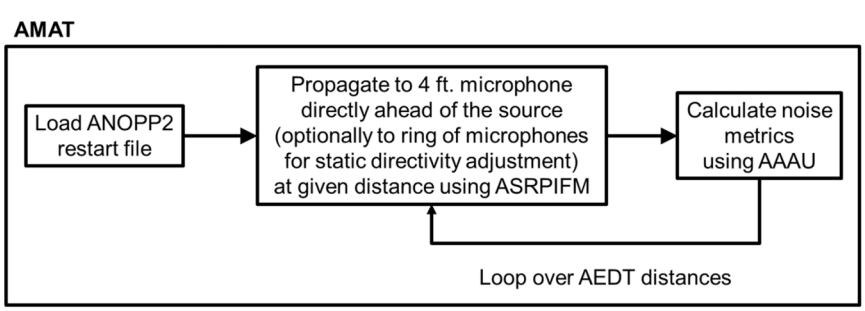

Fig. 13 Computational steps in AMAT for generating rotary-wing NPD data for static operational modes G, H, I, and J.

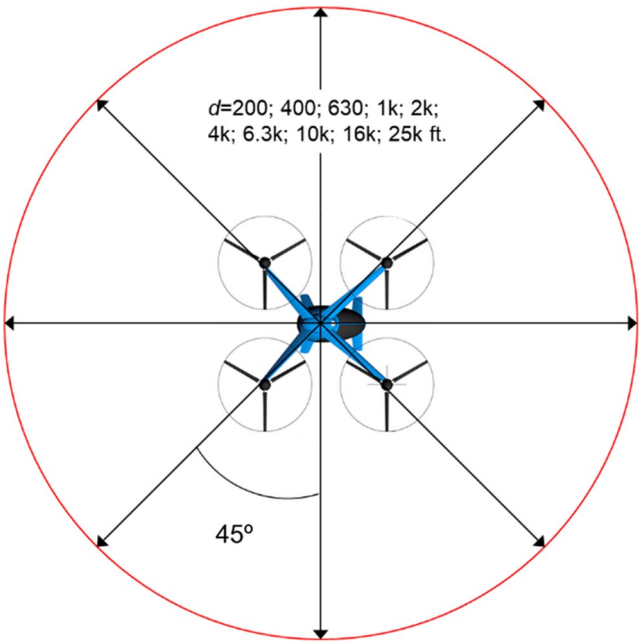

Fig. 14 Static directivity adjustment data collection points for operational modes G, H, I, and J.

b. Static Modes I (Hover in Ground Effect) and J (Hover out of Ground Effect). The methods for calculating NPD data for modes I and J are the same; it is only the source noise data that differ. Within AEDT, the selection of mode I and J (as well as modes V and W, and modes Y and Z) is dictated by the ground effect altitude (in feet above field elevation), which is equal to 1.5 times the main rotor diameter for helicopters. If the procedural step is below the ground effect altitude, operational mode I (V and Y) will be used. Otherwise, operational mode J (W and Z) will be used. Because the applicability of the "helicopter ground effect altitude" criterion for UAM vehicles is questionable, only NPD data for mode J are calculated. When mode I is required within AEDT, it is provided by substitution (see Table 2). The operating state of zero airspeed and zero climb angle is used for mode J (see Fig. 2). The corresponding source noise data were obtained with the ground effect model of CAMRAD II disabled.

Lacking a standard, mode J NPD data are calculated at a cone angle between 30 and 45°. The cone angle is the angle between the horizon and the observers that compose a circle of locations centered below the vehicle. For this calculation, the source noise hemisphere is positioned at an altitude equal to the AEDT reference distance times the sine of the cone angle. Source directivity data are obtained in 15–45° increments.

V. Simulated NPD Data

In this section, NPD data obtained via simulation are provided for fixed-wing and rotary-wing modes, and comparisons are made where appropriate. International Standard Atmosphere conditions at sea level (1 atm pressure, 59°F [15°C] temperature, and 0.076 lb/ft^3 [1.225 kg/m^3] air density) and 70% relative humidity were used throughout the tool chain. In the simulations, a flow resistivity of 250k MKS Rayls, corresponding to grass, was used for the soft ground impedance. Tabularized fixed-wing and rotary-wing NPD data are provided in the Supplemental Material that accompany this paper (see Appendix).

A. Fixed-Wing Aircraft

A comparison of simulated L_{AE} data, incorporating periodic loading and thickness noise and broadband noise, is shown in Fig. 15 for the quadrotor and L+C vehicles. Different colors are used for each airspeed increment. Here it is seen that, for cruise conditions, the quadrotor vehicle has higher levels than the L+C vehicle, as it does not benefit from lift generated by a wing. In contrast, the L+C vehicle has higher levels on takeoff and climb (departure), and, to a lesser extent, for higher speed descent conditions (approach) compared to the quadrotor vehicle. This is more clearly seen over the full range of AEDT distances in Fig. 16 for a departure and cruise condition. Plots of the other metrics appear similar and are omitted for brevity.

B. Rotary-Wing Aircraft

1. Dynamic Operational Modes

a. Dynamic Mode L (Level Flyover at Constant Speed). Mode L NPD data were simulated for all quadrotor operating states with zero climb angle. L_{AE} data are shown in Fig. 17 for centerline and 45° port-side microphone locations. In these and subsequent mode L, D, and A plots, the legend designates the airspeed V in knots and the climb angle A in degrees. The aims of plotting all data on a single plot are i) to identify trends and the spread in the data between operating states and microphone locations and ii) to identify outliers. For both locations in Fig. 17, the data are clustered within a range of about 3 dBA. Centerline levels are considerably higher than port-side levels. Starboard-side data are similar to port-side data and are omitted for brevity.

Mode L NPD data were simulated for all L+C high-speed operating states, inclusive of those with positive (departure) and negative (approach) climb angles. This was motivated by the observation that the high-speed positive and negative climb angle data are closer in level to the high-speed zero-degree-climb-angle data than they are to the departure and approach conditions in the low-speed and moderate-speed regimes (see Fig. 15). L_{AE} data are shown in Fig. 18 for centerline and 45° port-side microphone locations. The L+C plots carry the additional designation in the legend for low-speed (LS),

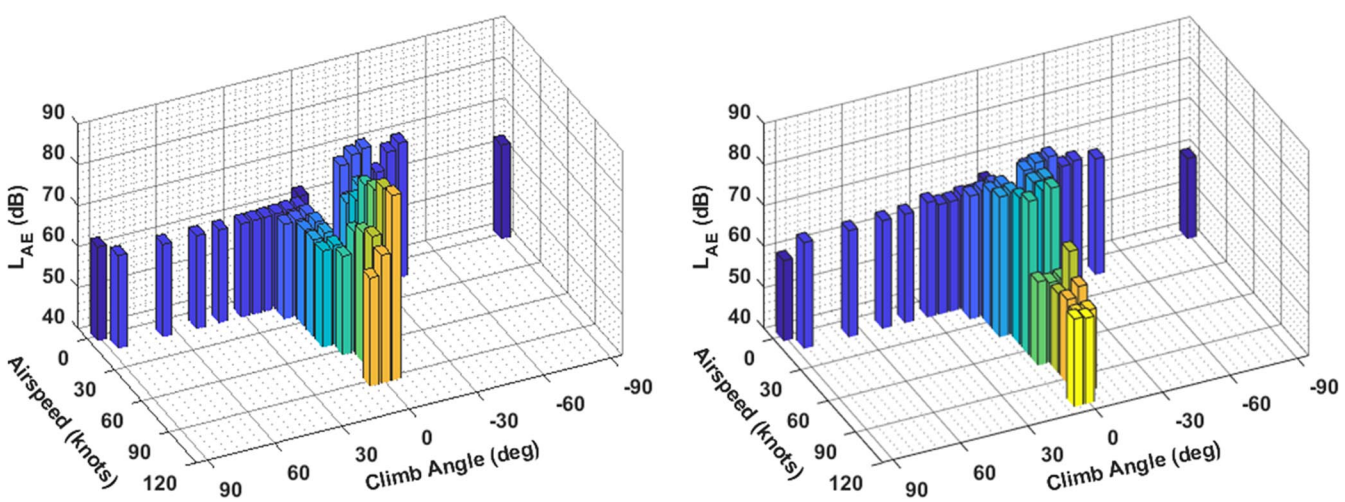

Fig. 15 Simulated fixed-wing L_{AE} data for the quadrotor (left) and L+C (right) at $d = 1000$ ft (305 m).

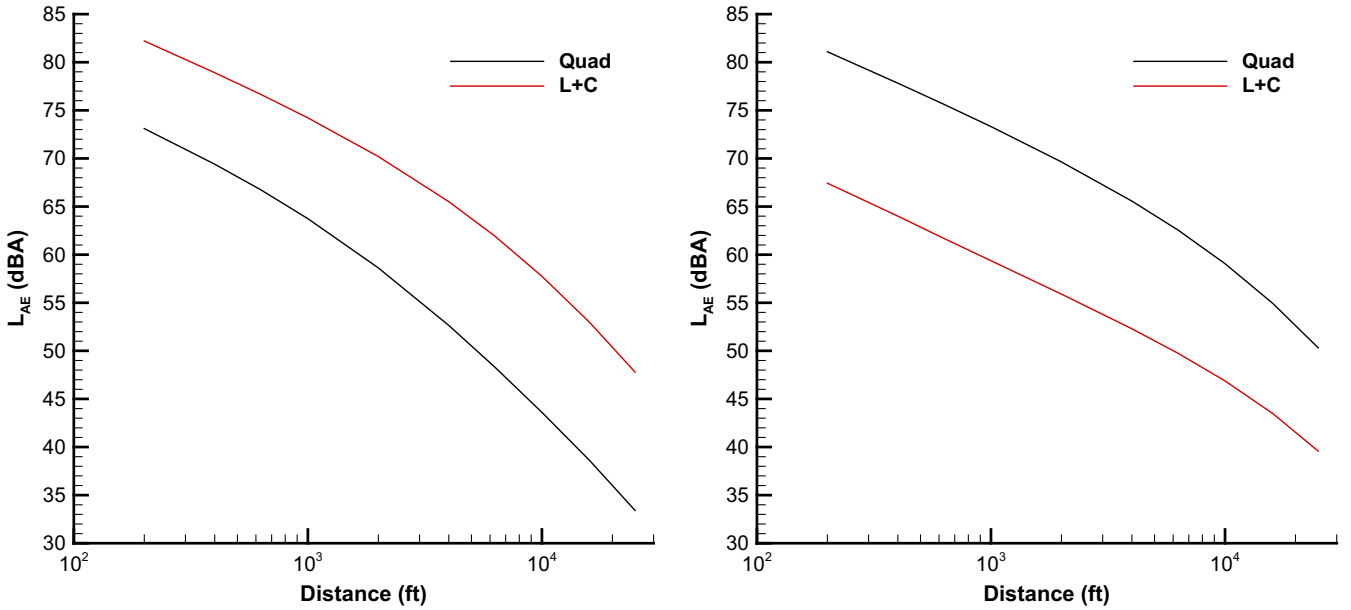

Fig. 16 Simulated fixed-wing L_{AE} data for a departure operating state (40 knots, 10° climb angle) (left) and a cruise operating state (80 knots, 0° climb angle) (right).

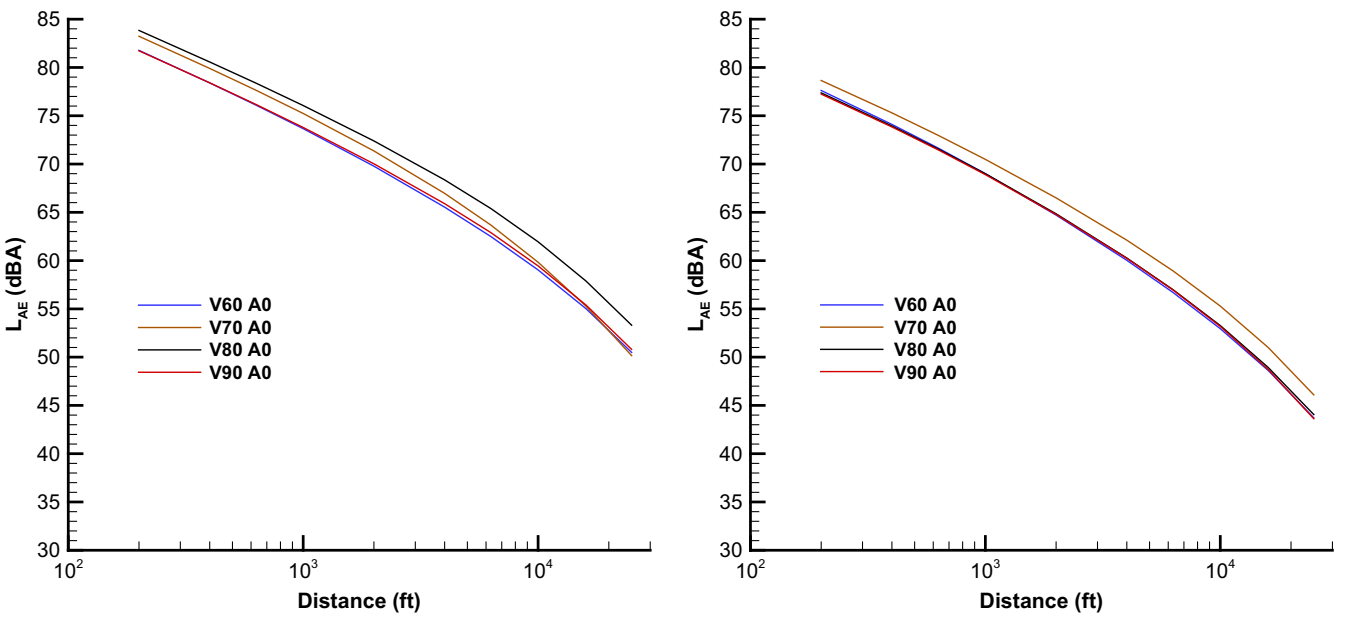

Fig. 17 Simulated mode L L_{AE} data for quadrotor vehicle at centerline (left) and 45° port-side (right) microphone locations.

moderate-speed (MS), and high-speed (HS) trim states (see Sec. III.A). With the exception of the 80- and 90-knot conditions at the −5° climb angle, the data are also clustered within a range of about 3 dBA for both locations. Centerline levels are marginally higher than port-side levels.

The regression for the advancing tip Mach number adjustment, using only the level flyover operating states, is shown in Fig. 19 for the quadrotor and L+C vehicles. According to guidance issued by the U.S. Department of Transportation, Volpe National Transportation Systems Center, if the second-order polynomial regression given by Eq. (1) is not in the form of an upward curve that increases with increasing ΔM_{ADV}, then a linear regression should be used. This was the case for all three microphone locations for the quadrotor, and for the centerline microphone for the L+C. Regression coefficients are provided in Table 3. The selection of reference airspeeds of 90 knots (167 km/h) and 110 knots (204 km/h) for the quadrotor and L+C vehicles, respectively, was based on the observation in Ref. [6] that most of the time at cruise was spent at these conditions. The nonzero value of ΔM_{ADV} at the reference speed is due to the difference in temperature between the reference temperature of 77°F (25°C) and the operational temperature of 59°F (15°C). In the case of the L+C, because the level flight operating states are fully propeller driven, the rotational blade tip Mach number contribution to M_{ADV} in Eq. (2) is zero. The simulated data for the quadrotor are symmetric with respect to the centerline. The levels are somewhat higher on the left (port) side than the right (starboard) side for the L+C vehicle because the nose is pitched up in level flight, and the direction of the pusher propeller rotation is counterclockwise looking forward. Therefore, the left (advancing) side has a somewhat higher tip Mach number than the starboard (right) retreating side, giving slightly higher levels on the port side.

The effectiveness of this condensation can be evaluated by applying the adjustment at the appropriate ΔM_{ADV} to the data at the reference airspeed. Figure 20 compares the simulated L_{AE} data at all level flyover airspeeds with the L_{AE} data at the reference airspeed adjusted for the advancing tip Mach number, the latter being the values used within AEDT. The error between the simulated data and

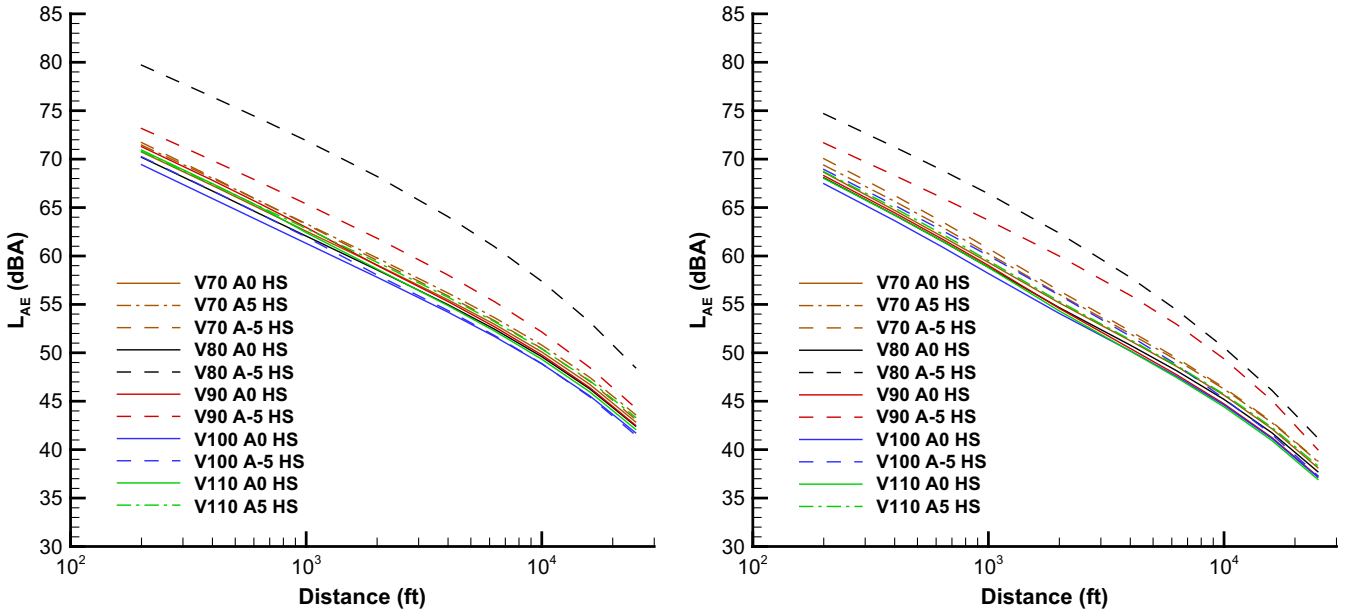

Fig. 18 Simulated mode L L_{AE} data for L+C vehicle in high-speed conditions at centerline (left) and 45° port-side (right) microphone locations.

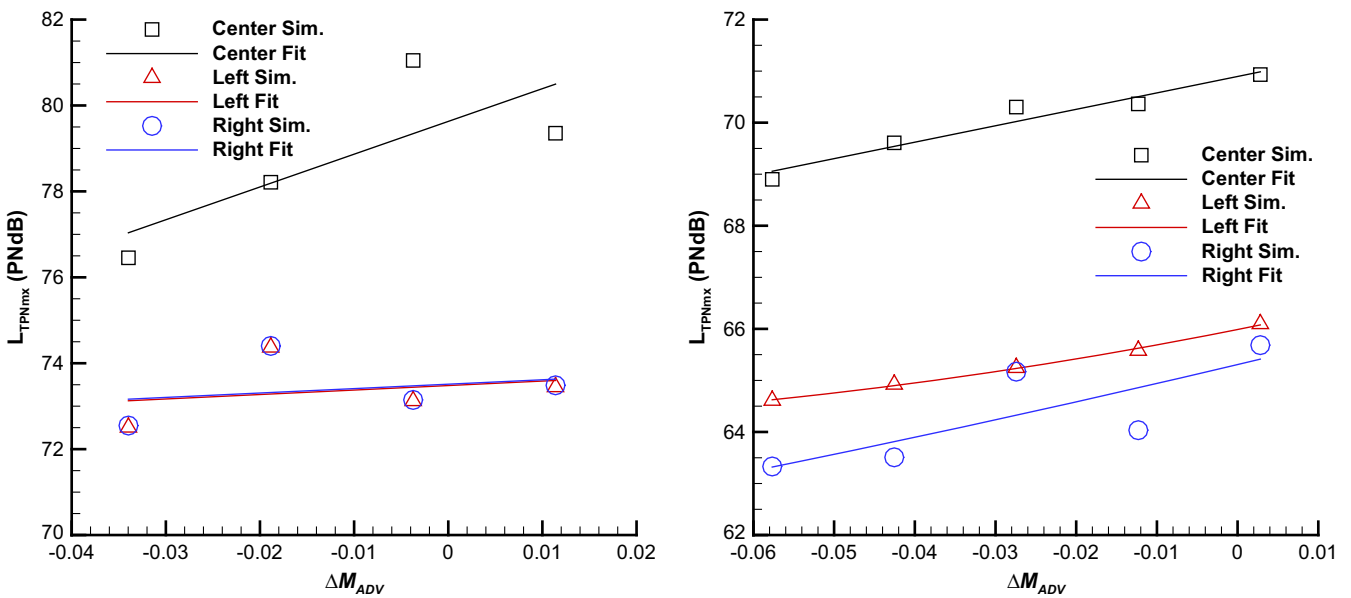

Fig. 19 Regression of simulated mode L L_{TPNmx} data at $d = 1000$ ft (305 m) for the advancing tip Mach number adjustment of quadrotor (left) and L+C (right) vehicles.

Table 3 Regression coefficients for the advancing tip Mach number adjustment

Microphone location	Quadrotor			Lift plus cruise		
	B_0	B_1	B_2	B_0	B_1	B_2
Center	79.63	76.28	0	70.90	31.88	0
Left	73.48	10.42	0	65.99	31.15	130.4
Right	73.51	10.28	0	65.31	37.13	45.86

the adjusted data is lowest at the reference point and generally increases with increasing ΔM_{ADV}.

An alternative condensation scheme is to select a single-level flyover operating state (at the reference airspeed) and use those data for all level flyover operating states. This is the only available condensation method for modes D and A. Which of the two condensation schemes is most effective is largely dependent on the particular flight route(s) being evaluated.

b. Dynamic Mode D (Departure at Constant Speed). Mode D NPD data were simulated for all operating states with positive climb angles of 5, 10, and 15°. The limitation on climb angles above 15° was made to ensure that the advancing side 10 dB down point needed for noise exposure metrics is met for the shorter AEDT reference distances. This is a conservative estimate made on the assumption of a monopole source and spherical spreading loss only. In the intended application, the higher climb angles will be cast as vertical ascent modes V/W, which will be substituted per Table 2 for hover modes I/J within AEDT.

Simulated mode D L_{AE} data for the quadrotor vehicle are shown in Fig. 21 for centerline and 45° port-side microphone locations. For both locations in Fig. 21, the data are clustered within a range of about 9 dBA. Centerline levels are marginally higher than port-side levels. Starboard-side data are similar to port-side data and are omitted for brevity. There is some crossover of NPD data with range, making selection of a low noise and high noise case range-dependent.

Simulated mode D L_{AE} data for the L+C vehicle operating in the low- and moderate-speed regimes are shown in Fig. 22 for centerline

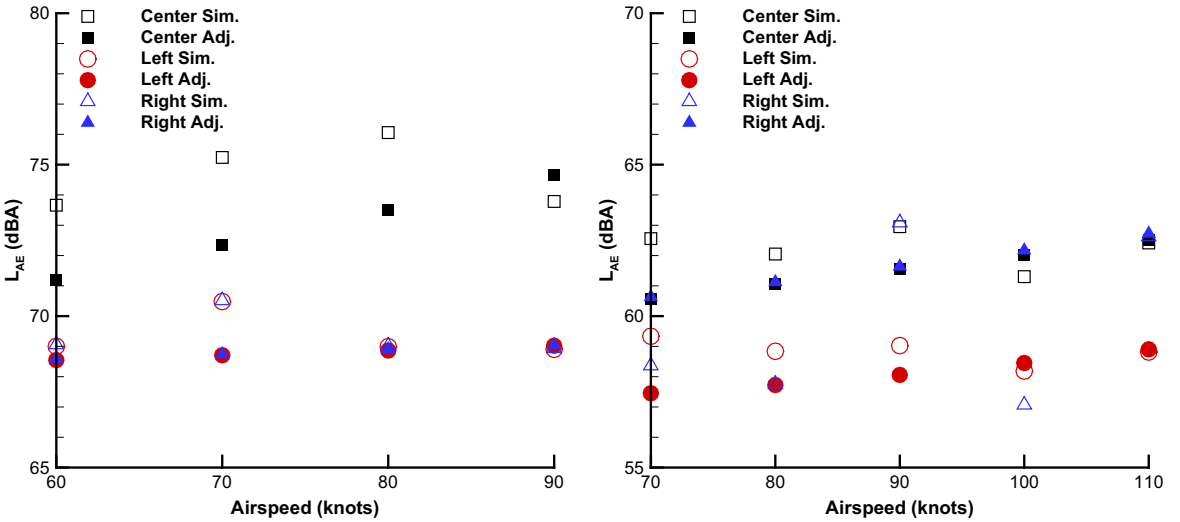

Fig. 20 Simulated mode L L_{AE} data at $d = 1000$ ft (305 m) with reference airspeed data adjusted for advancing tip Mach number for quadrotor (left) and L+C (right) vehicles.

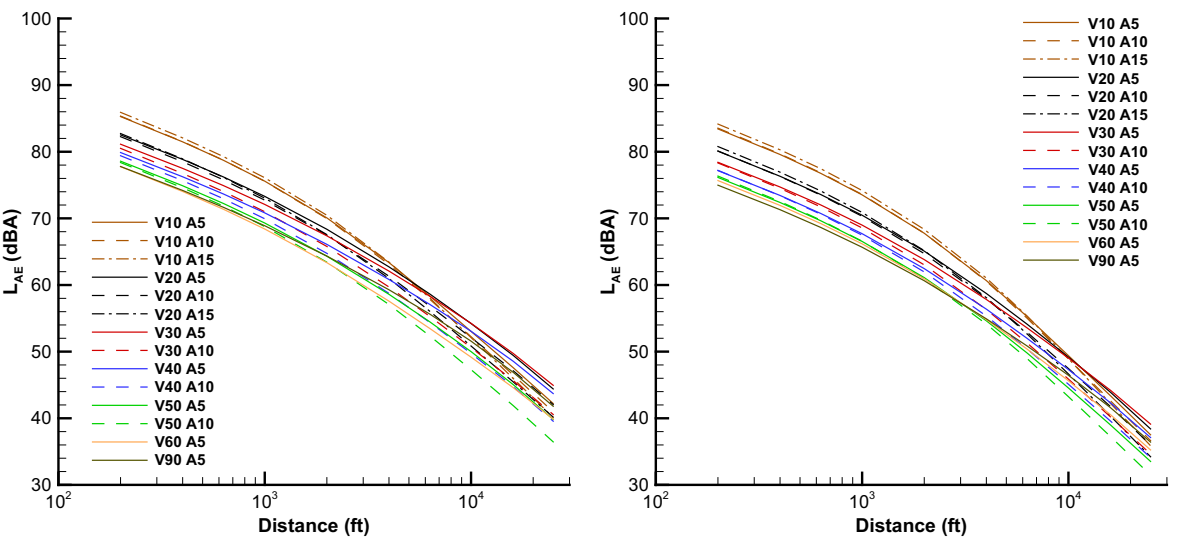

Fig. 21 Simulated mode D L_{AE} data for quadrotor vehicle at centerline (left) and 45° port-side (right) microphone locations.

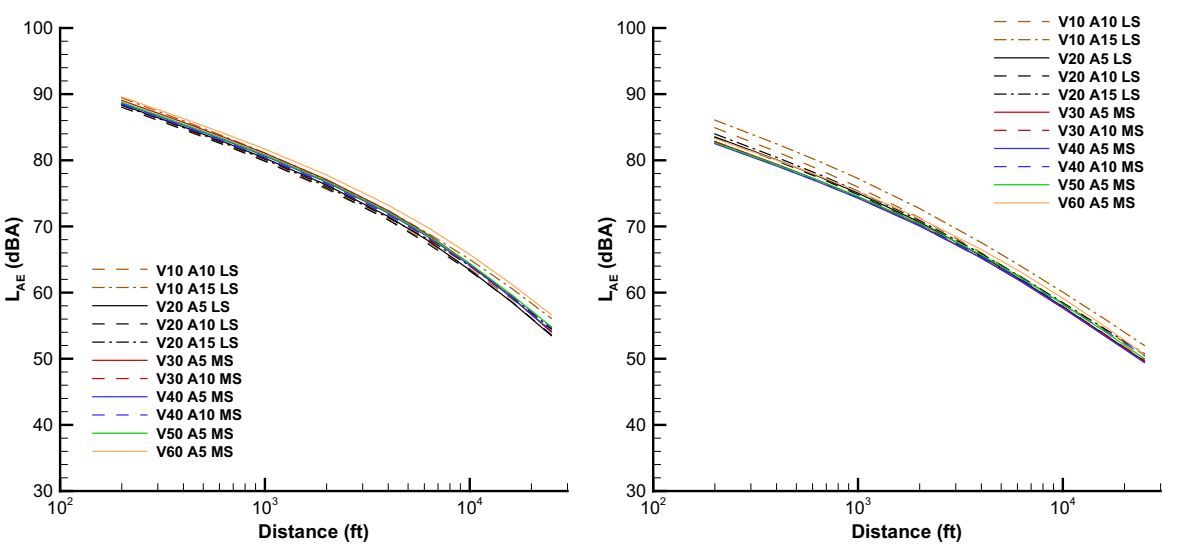

Fig. 22 Simulated mode D L_{AE} data for L+C vehicle in low and moderate speed conditions at centerline (left) and 45° port-side (right) microphone locations.

and 45° port-side microphone locations. In comparison to the quadrotor vehicle, the L+C levels are higher and more tightly clustered, with a spread of about 2 dBA, at the low- and moderate-speed states.

c. Dynamic Mode A (Approach at Constant Speed). For a similar consideration as mode D, mode A NPD data were simulated for all operating states with descent angles 5, 10, and 15°. Within AEDT, the higher descent angles will be cast as vertical descent modes Y/Z, which will be substituted per Table 2 for hover modes I/J.

Simulated L_{AE} data for mode A for the quadrotor vehicle are shown in Fig. 23 for centerline and 45° port-side microphone locations. In comparison to the mode D data, the mode A data are at higher levels due to induced blade–vortex interaction noise in descent. While the data are mostly parallel, the spread between the low and high noise conditions is about 12 dBA. This large range will lead to significant inaccuracies in AEDT noise exposure estimates when a single mode A data set is chosen.

Simulated mode A L_{AE} data for the L+C vehicle are shown in Fig. 24 for centerline and 45° port-side microphone locations. Although the levels are somewhat higher than the mode D operating conditions in Fig. 22, they are still lower than those of the quadrotor vehicle. Further, because they are mostly parallel and with a small spread, selection of a single curve that represents all mode A operating states is straightforward and will not introduce much inaccuracy in AEDT noise exposure estimates.

2. Static Operational Modes

a. Static Mode H (Flight Idle). A comparison of simulated L_{Amx} data directly ahead of both vehicles is shown in Fig. 25. The data were computed at a 0° elevation angle. The noise produced by the lifting rotors of the L+C vehicle is seen to exceed that of the quadrotor vehicle; the latter falls below 0 dBA at the 16k and 25k ft (4.88 and 7.62 km) reference distances. While there is no fixed-wing analog to this operational mode, the higher level of the L+C vehicle is consistent with the 0 knot, 0°-climb-angle operating state. The kink in the

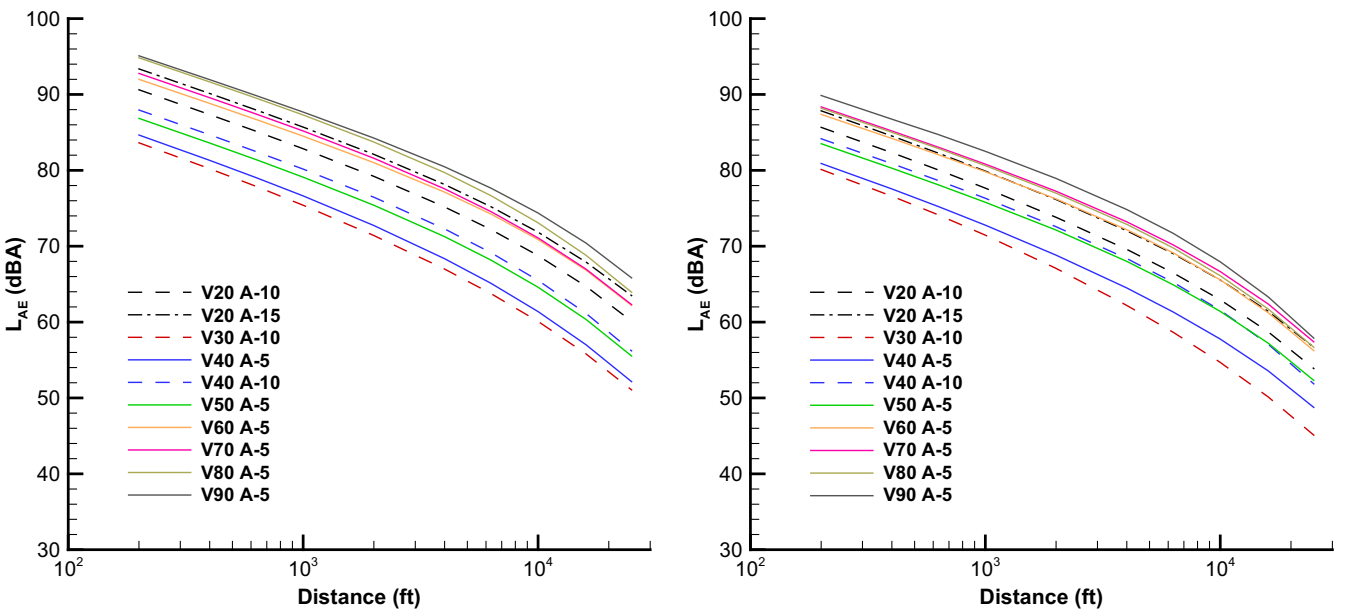

Fig. 23 Simulated mode A L_{AE} data for quadrotor vehicle at centerline (left) and 45° port-side (right) microphone locations.

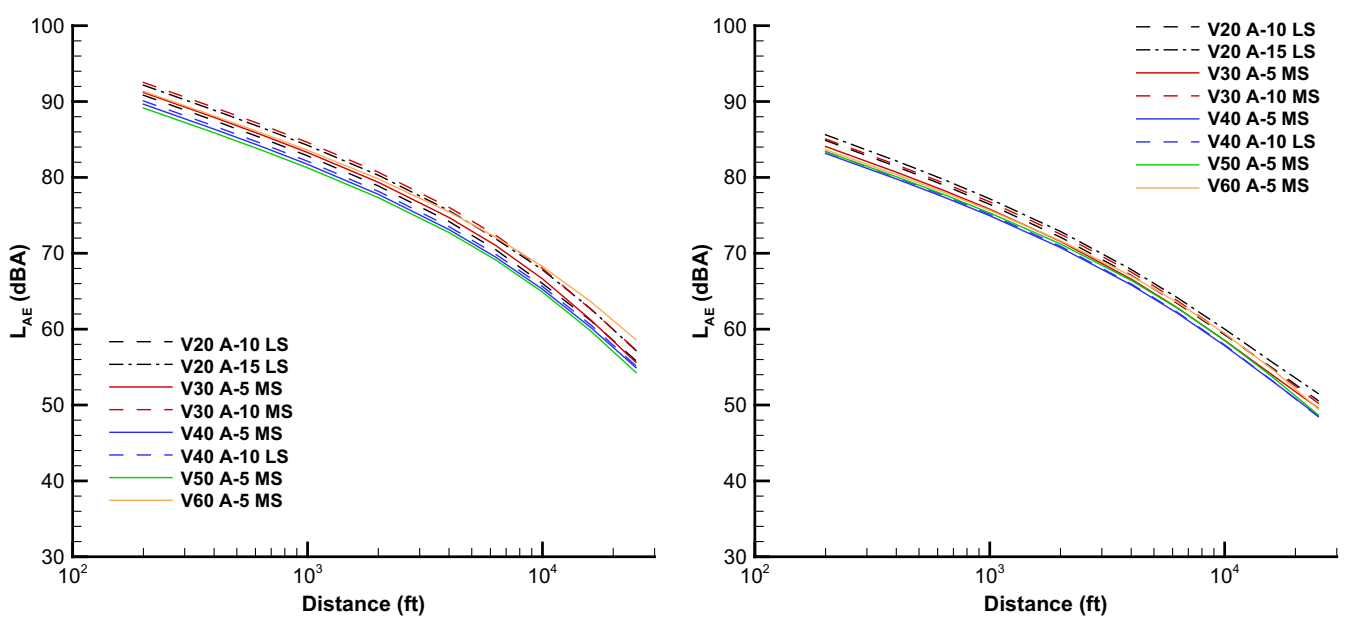

Fig. 24 Simulated mode A L_{AE} data for L+C vehicle in low and moderate speed conditions at centerline (left) and 45° port-side (right) microphone locations.

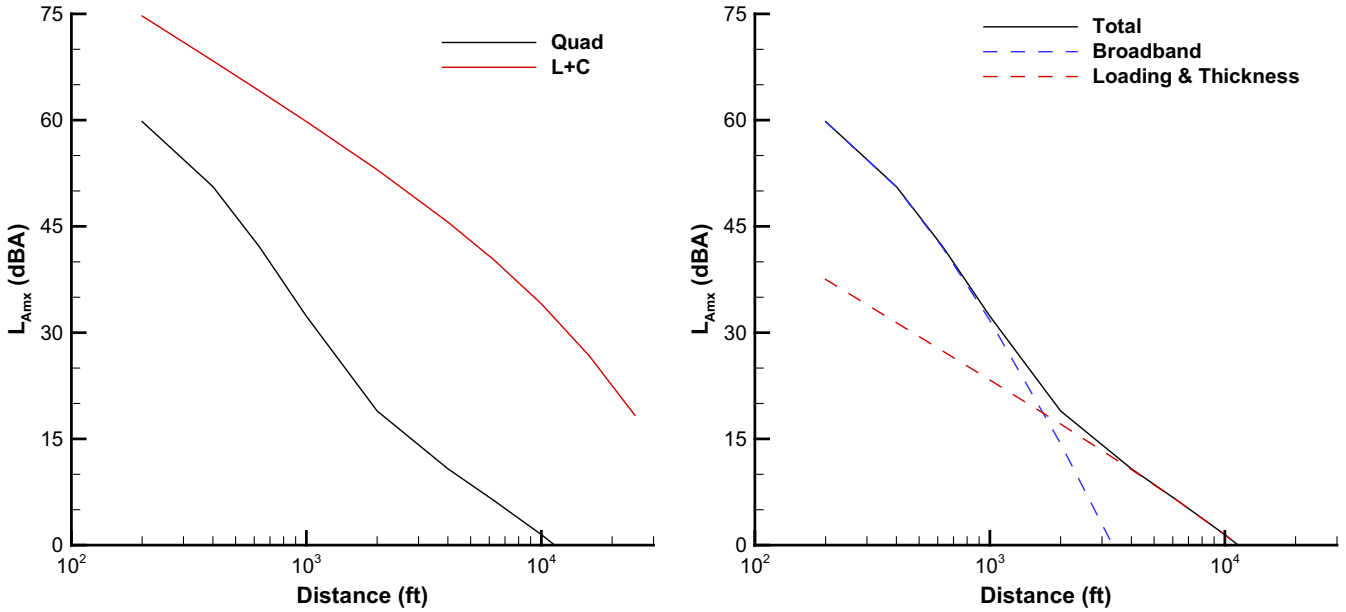

Fig. 25 Simulated mode H L_{Amx} data directly ahead of quadrotor and L+C vehicles (left) and quadrotor component noise source contributions (right).

quadrotor vehicle curve at the 2k ft (610 m) reference distance is attributable to changes in the component source noise contributions with distance. At short distances, the quadrotor noise ahead of the vehicle is dominated by the high-frequency broadband self-noise component, while at longer distances, the noise is dominated by the lower frequency loading and thickness noise components, as shown in Fig. 25. The loading and thickness noise of the L+C ahead of the vehicle dominates over the broadband self-noise component at all reference distances (not shown). These relative contributions differ at other azimuthal angles.

The static directivity of the quadrotor vehicle is shown in Fig. 26. The nose of the vehicle is at 0° and the pattern is practically symmetric about the body axis. The adjustments relative to the 0° data are also shown in Fig. 26. The spikey appearance of the adjustments is accentuated by the 15° resolution used for AEDT. While the directivity shape does not vary much with distance, the adjustment levels increase with increasing distance. This indicates that the recommended directivity distance of 200 ft (61 m) substantially underestimates the adjustments at the remaining distances, particularly those above 1000 ft (305 m).

In contrast, the static directivity levels for the L+C vehicle, shown in Fig. 27, are higher in amplitude. Up to 2000 ft (610 m), the adjustments maintain a similar shape but vary in level by about 2 dB (between about 6 and 8 dB). At greater distances, the adjustments change in shape and level as the directivity increasingly flattens laterally relative to that fore and aft due to differences in the spectral balance.

b. Static Mode J (Hover out of Ground Effect). A comparison of L_{Amx} data directly ahead of both vehicles is shown in Fig. 28 for static mode J. The data were computed at a cone angle of 30°, in the lower hemisphere region with a generally higher broadband self-noise component than found at 0°. Consistent with Fig. 15, the L+C levels exceed those of the quadrotor for this condition.

The static directivity pattern and adjustments, shown in Fig. 29 for the quadrotor vehicle, are again practically symmetric about the body axis. While the directivity shape does not vary much with distance, the adjustment levels increase with increasing distance, consistent with a spectral balance dominated by high-frequency broadband self-noise. The recommended directivity distance of 200 ft (61 m) again substantially underestimates the adjustments at the remaining distances, particularly those in excess of 1000 ft (305 m). The static directivity pattern and adjustments for the L+C vehicle are shown in Fig. 30.

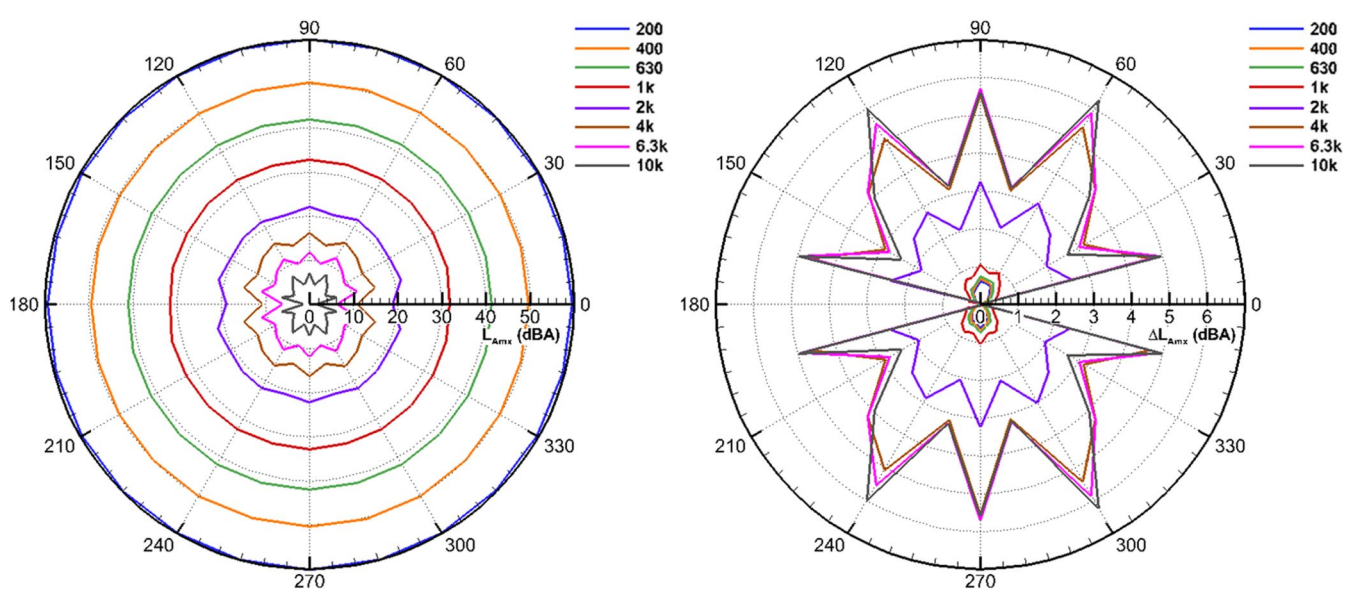

Fig. 26 Mode H static directivity L_{Amx} (left) and adjustments relative to 0° ΔL_{Amx} (right) for the quadrotor vehicle.

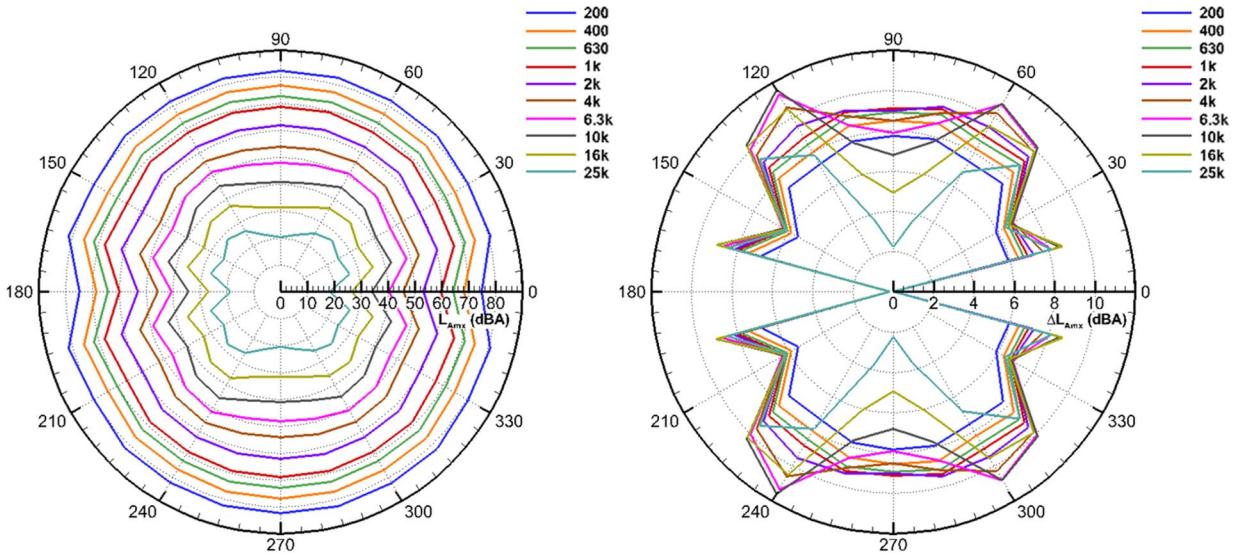

Fig. 27 Mode H static directivity L_{Amx} (left) and adjustments relative to 0° ΔL_{Amx} (right) for the L+C vehicle.

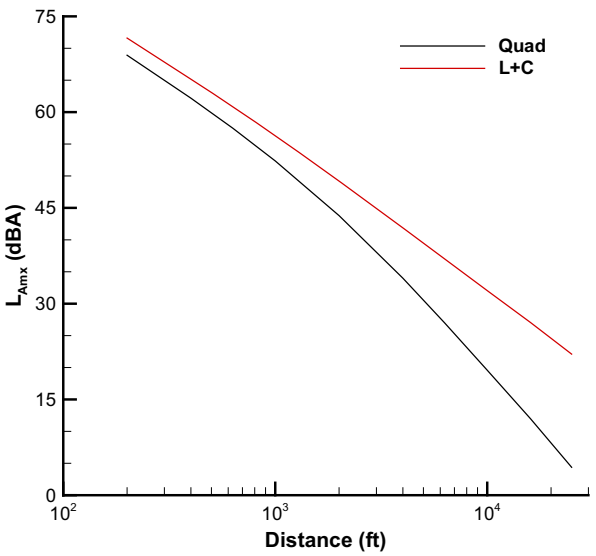

Fig. 28 Simulated mode J L_{Amx} data directly ahead of quadrotor and L+C vehicles.

The adjustment levels are larger than those of the quadrotor at every distance.

VI. Conclusions

Methods were presented for generating fixed-wing and rotary-wing NPD data from predictions of UAM vehicle source noise. The data are intended for use in studies of community noise impact from UAM flight operations. The fixed-wing NPD data are intended for use in Doc 9911–compliant computer programs, including AEDT. The rotary-wing NPD data are intended specifically for use in AEDT. Generation of these data in this manner was necessitated by several factors, including lack of UAM aircraft noise and performance data in the databases used by integrated noise modeling tools, including AEDT, and a general lack of measured UAM flight test data.

Predictions of periodic loading and thickness noise and broadband self-noise were made for two reference concept vehicles that were trimmed for a range of operating states using a framework that included a comprehensive analysis code for trim and the NASA ANOPP2 for acoustic analyses. The resulting noise hemispheres served as input to a simulation tool for generating both fixed-wing and rotary-wing NPD data, allowing the vehicles to be

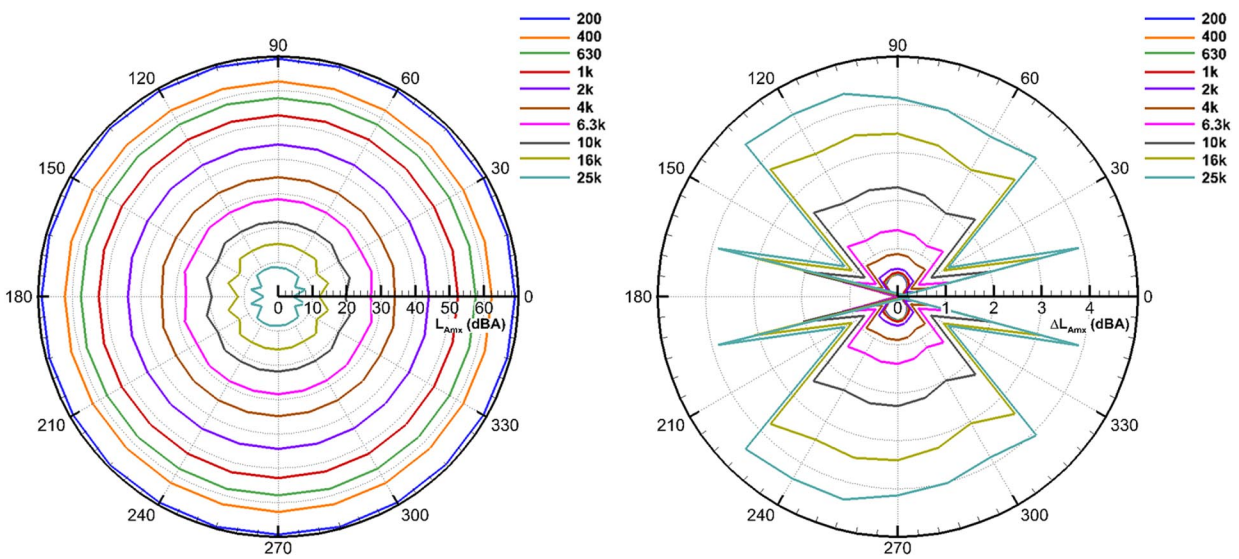

Fig. 29 Mode J static directivity L_{Amx} (left) and adjustments relative to 0° ΔL_{Amx} (right) for the quadrotor vehicle.

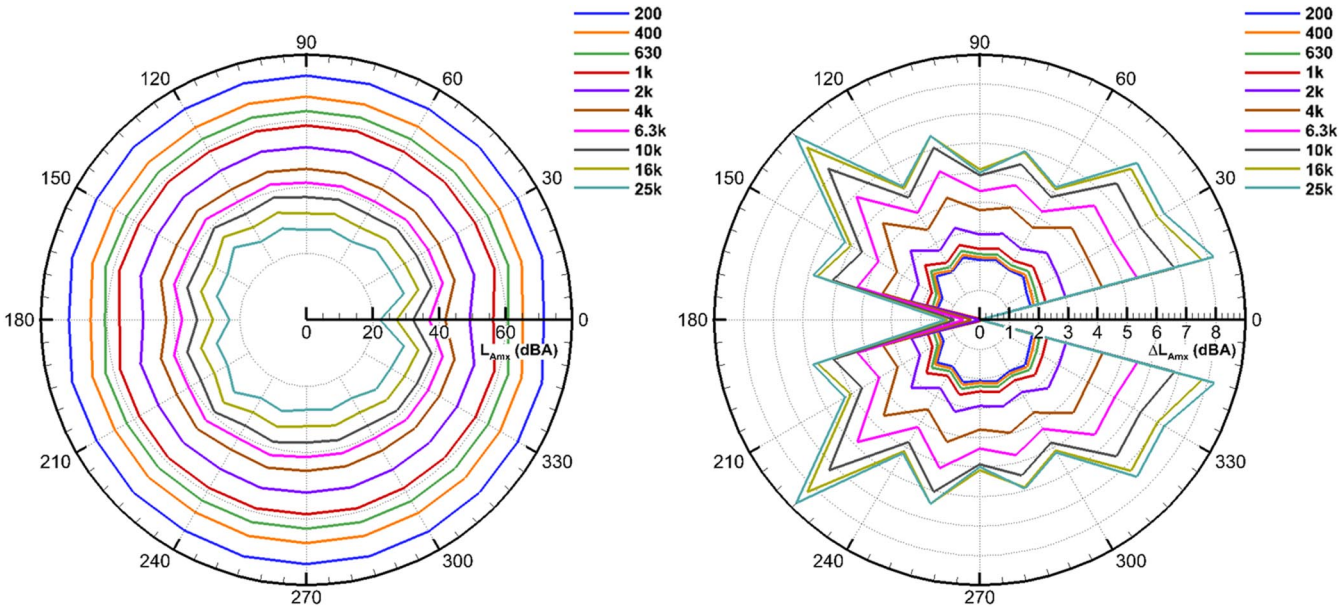

Fig. 30 Mode J static directivity L_{Amx} (left) and adjustments relative to 0° ΔL_{Amx} (right) for the L+C vehicle.

modeled in different ways. Given that most integrated noise modeling tools, including AEDT, were originally developed for near-airport operations and not for point-to-point operations, the ability to assess noise exposure via alternative means is key to identifying best modeling practices. To that end, work is underway to compare AEDT modeling results using fixed-wing, rotary-wing, and hybrid fixed/rotary-wing approaches with simulation data.

The computational framework developed herein is extensible and allows the inclusion of other noise sources, e.g., electric motor noise and other forms of interaction noise, in the future. It is robust in that it is not limited to the two vehicle configurations considered in this work. The generation of NPD data for other advanced air mobility vehicle configurations including vectored thrust (tilt-rotor and tilt-wing) is entirely possible. This capability allows assessments of community noise exposure to be performed well in advance of the introduction of services and is essential for the siting of vertiports and the development of low-noise routes.

Appendix: Description of Supplemental Material

Generation 3.1.2 source noise and NPD data are provided as Supplemental Material with this paper. For each reference vehicle, source noise hemisphere data containing combined periodic loading and thickness noise and broadband self-noise are provided as one-third octave band spectra in ASCII-formatted files for each operating state. For each reference vehicle, fixed-wing NPD data for each operating state and rotary-wing NPD data for modes L, A, D, H, and J are provided in ASCII-formatted files. A detailed listing is provided as part of the Supplemental Material.

Acknowledgments

This work was supported by the NASA Aeronautics Research Mission Directorate, Revolutionary Vertical Lift Technology Project. The authors wish to acknowledge Venkat Iyer (Analytical Sciences and Materials, Inc.) and Jeremy Jones (Analytical Mechanics Associates, Inc.) for development of the ANOPP2 Mission Analysis Tool (AMAT) used in this work. The authors also wish to thank Eric Boeker and Bradley Nicholas of the U.S. Department of Transportation Volpe National Transportation Systems Center for their consultation during the development of the methodology discussed in this paper.

References

[1] *Doc 9911, Recommended Method for Computing Noise Contours Around Airports*, 2nd ed., International Civil Aviation Organization, Montreal, 2018, pp. 1–198.

[2] "ECAC.CEAC Doc 29, Report on Standard Method of Computing Noise Contours Around Civil Airports, Volume 2: Technical Guide," 4th ed., *European Civil Aviation Conference–Conférence Européenne De L'Aviation Civile*, International Civil Aviation Organization (ICAO) and The Council of Europe, 2016, pp. 1–139, https://en.wikipedia.org/wiki/European_Civil_Aviation_Conference.

[3] "Aviation Environmental Design Tool (AEDT) Technical Manual, Version 3e," U.S. Department of Transportation, Volpe National Transportation Systems Center, MA DOT-VNTSC-FAA-22-04, Cambridge, MA, 2022.

[4] Rizzi, S. A., Huff, D. L., Boyd, D. D., Jr., Bent, P., Henderson, B. S., Pascioni, K. A., Sargent, D. C., Josephson, D. L., Marsan, M., He, H., and Snider, R., "Urban Air Mobility Noise: Current Practice, Gaps, and Recommendations," NASA TP-2020-5007433, 2020.

[5] Lopes, L. V., and Burley, C. L., "ANOPP2 User's Manual: Version 1.2," NASA TM-2016-219342, 2016.

[6] Rizzi, S. A., and Rafaelof, M., "Community Noise Assessment of Urban Air Mobility Vehicle Operations Using the FAA Aviation Environmental Design Tool," *InterNoise 2021*, Paper IN-2021-1482, Inst. of Noise Control Engineering, 2021. https://doi.org/10.3397/IN-2021-1482

[7] Rizzi, S. A., and Rafaelof, M., "Second Generation UAM Community Noise Assessment Using the FAA Aviation Environmental Design Tool," *AIAA SciTech Forum*, AIAA Paper 2022-2167, 2022. https://doi.org/10.2514/6.2022-2167

[8] Patterson, M. D., Antcliff, K. R., and Kohlman, L. W., "A Proposed Approach to Studying Urban Air Mobility Missions Including an Initial Exploration of Mission Requirements," *AHS International 74th Annual Forum and Technology Display*, American Helicopter Soc. Paper 74-2018-0185, 2018.

[9] Silva, C., Johnson, W. R., Solis, E., Patterson, M. D., and Antcliff, K. R., "VTOL Urban Air Mobility Concept Vehicles for Technology Development," *AIAA Aviation Forum*, AIAA Paper 2018-3847, 2018. https://doi.org/10.2514/6.2018-3847

[10] Johnson, W. R., "Rotorcraft Aerodynamic Models for a Comprehensive Analysis," *AHS International 54th Annual Forum*, American Helicopter Soc. Paper 54-00103, 1998.

[11] Farassat, F., and Succi, G., "The Prediction of Helicopter Rotor Discrete Frequency Noise," *Vertica*, Vol. 7, 1983, pp. 309–320.

[12] Lopes, L. V., "ANOPP2's Farassat Formulations Internal Functional Modules (AFFIFMs) Reference Manual, Version 1.4," NASA TM-20210021111, 2021.

[13] Lopes, L. V., "Compact Assumption Applied to Monopole Term of Farassat's Formulations," *Journal of Aircraft*, Vol. 54, No. 5, 2017, pp. 1649–1663. https://doi.org/10.2514/1.C034048

[14] Brooks, T. F., Pope, D. S., and Marcolini, M. A., "Airfoil Self-Noise and Prediction," NASA RP-1218, 1989.

[15] Johnson, W. R., "NDARC—NASA Design and Analysis of Rotorcraft: Validation and Demonstration," *American Helicopter Society Specialists' Conference on Aeromechanics*, American Helicopter Soc., 2010.

[16] van der Wall, B. G., "2nd Higher Harmonic Control (HHC) Aeroacoustic Rotor Test (HART II)–Part I: Test Documentation," German Aerospace Center (DLR) IB 111-2003/31, 2003.

[17] Synodinos, A. P., Self, R. H., and Torija, A. J., "Framework for Predicting Noise–Power–Distance Curves for Novel Aircraft Designs," *Journal of Aircraft*, Vol. 55, No. 2, 2018, pp. 781–791. https://doi.org/10.2514/1.C034466

[18] "Aircraft Noise and Performance (ANP) Data," Ver. 2.3, https://www.easa.europa.eu/en/domains/environment/policy-support-and-research/aircraft-noise-and-performance-anp-data/anp-legacy-data [retrieved 15 Aug. 2023].

[19] "User Manual for the Base of Aircraft Data (BADA) Revision 3.6," Eurocontrol Experimental Centre, EEC Note No. 10/04, Brétigny-sur-Orge, France, July 2004.

[20] "Standard Values of Atmospheric Absorption as a Function of Temperature and Humidity," SAE ARP 866 Rev. A, SAE International, Warrendale, PA, 1975, https://www.sae.org/standards/content/arp866a/.

[21] Chien, C. F., and Soroka, W. W., "Sound Propagation Along an Impedance Plane," *Journal of Sound and Vibration*, Vol. 43, No. 1, 1975, pp. 9–20. https://doi.org/10.1016/0022-460X(75)90200-X

[22] Delany, M. E., and Bazley, E. N., "Acoustical Properties of Fibrous Absorbent Materials," *Applied Acoustics*, Vol. 3, No. 2, April 1970, pp. 105–116. https://doi.org/10.1016/0003-682X(70)90031-9

[23] "Procedure for the Calculation of Airplane Noise in the Vicinity of Airports," SAE AIR 1845 Rev. A, SAE International, Warrendale, PA, 2012, https://www.sae.org/standards/content/air1845a/.

[24] "Part 36—Noise Standards: Aircraft Type and Airworthiness Certification, Appendix H–Noise Requirements for Helicopters Under Subpart H," United States Code of Federal Regulations, 2016, https://www.ecfr.gov/current/title-14/part-36.

[25] Rickley, E. J., Jones, K. E., Keller, A. S., and Fleming, G. G., "Noise Measurement Flight Test of Five Light Helicopters," U.S. Department of Transportation, Volpe National Transportation Systems Center DOT-VNTSC-FAA-93-5, Cambridge, MA, 1993.

[26] Rizzi, S. A., and Rafaelof, M., "On the Modeling of UAM Aircraft Community Noise in AEDT Helicopter Mode," *2023 AIAA Aviation Forum*, AIAA Paper 2023-3363, 2023. https://doi.org/10.2514/6.2023-3363